

Fatigue of SFRC in compression: Size effect & autogenous self-healing

 G. Ruiz^a ,  Á. De La Rosa^b,  J.J. Ortega^c,  E. Poveda^a,  R.C. Yu^a,
 M. Tarifa^d,  X.X. Zhang^e,  L. Garijo^f

a. ETSI Caminos, C. y P., Universidad de Castilla-La Mancha, (Ciudad Real, Spain)

b. DIMME, Grupo de Durabilidad e Integridad Mecánica de Materiales Estructurales, Universidad Rey Juan Carlos, (Móstoles, Spain)

c. ETSI Minas y Energía, Universidad Politécnica de Madrid, (Madrid, Spain)

d. ETSI Aeronáutica y del Espacio, Universidad Politécnica de Madrid, (Madrid, Spain)

e. El Minera e Industrial de Almadén, Universidad de Castilla-La Mancha, (Almadén, Spain)

f. ETS Ingeniería y Diseño Industrial, Universidad Politécnica de Madrid, (Madrid, Spain)

: gonzalo.ruiz@uclm.es

Received 4 October 2024

Accepted 10 November 2024

Available on line 11 December 2024

ABSTRACT: This review synthesizes prior research on size effect and autogenous self-healing in steel fiber-reinforced concrete (SFRC) under compressive fatigue. It explores the fatigue behavior of SFRC, focusing on fiber reinforcement's role in post-cracking toughness, crack propagation, and fatigue endurance. The review demonstrates that larger SFRC specimens have reduced fatigue lives, attributed to increased elastic energy driving microcrack growth, aligning with classical size effect theory. Additionally, it highlights autogenous self-healing, where fatigue-induced microcracks release occluded water, promoting rehydration and calcium carbonate precipitation, which enhances residual strength. The interaction between size effect, fiber content, and self-healing is examined, offering insights into improving SFRC's durability under cyclic loading. These findings have practical implications for designing SFRC structures subjected to compressive fatigue, such as wind turbine towers and railway slabs.

KEY WORDS: Compressive fatigue of steel fiber reinforced concrete (SFRC); Size and shape effects; Fatigue-induced autogenous self-healing.

Citation/Citar como: Ruiz G, de la Rosa Á, Ortega JJ, Poveda E, Yu RC, Tarifa M, Zhang XX, Garijo L. Fatigue of SFRC in compression: Size effect & autogenous self-healing. Mater. Construcc. 74(356):e356. <https://doi.org/10.3989/mc.2024.395724>

RESUMEN: *Fatiga del HRFA en compresión: Efecto de escala & autorreparación autógena.* Este artículo revisa investigaciones sobre el efecto de escala y la autorreparación autógena en el hormigón reforzado con fibras de acero (HRFA) bajo fatiga en compresión. Se centra en el papel de las fibras en la tenacidad postfisuración, la propagación de grietas y la resistencia a la fatiga. La revisión muestra que las probetas de mayor tamaño tienen vidas de fatiga reducidas debido a la mayor energía elástica que impulsa el crecimiento de microgrietas, en consonancia con la teoría clásica del efecto de escala. Además, destaca la autorreparación autógena, donde las microgrietas liberan agua ocluida, promoviendo la rehidratación y la precipitación de carbonato cálcico, lo cual mejora la resistencia residual. Se examina la interacción entre el efecto de escala, el contenido de fibras y la autorreparación, aportando ideas para mejorar la durabilidad del HRFA bajo carga cíclica en estructuras, por ejemplo, en torres de turbinas eólicas y placas ferroviarias.

PALABRAS CLAVE: Fatiga de hormigón reforzado con fibras de acero (HRFA) en compresión; Efectos de escala y forma; Autorreparación autógena inducida por fatiga.

Copyright: ©2024 CSIC. This is an open-access article distributed under the terms of the Creative Commons Attribution 4.0 International (CC BY 4.0) License.

1. INTRODUCTION

Concrete is a quasi-brittle material, meaning its fracture behavior is highly dependent on the size and shape of the structural element (1). This size effect is a critical factor in concrete's mechanical response, particularly because the energy released in the fracture process zone for a given crack increment varies with the size of the element, influencing both crack propagation and the stress at which failure occurs. Extensive research has established that concrete's strength generally decreases as the size of the element increases, even when the geometry remains consistent across different scales (1–5). This size effect complicates the direct application of strength data obtained from laboratory specimens to larger structural elements, as the experimentally measured strength is typically higher than the effective strength in real structural applications.

Compressive strength is the most widely used parameter for assessing concrete capacity, as concrete performs best under compressive loads. However, this property is also affected by the size effect. For large elements, compressive strength tends to a finite value, which is considered the intrinsic strength of the material (2).

While the size effect in concrete has been studied extensively under quasi-static loads, its influence on fatigue behavior, particularly under compressive fatigue, remains less explored. Given that concrete is primarily used in compression members in structures, understanding this relationship is crucial for predicting the long-term performance of concrete under cyclic loading.

Most research on the fatigue of concrete has focused on flexural behavior, examining crack propagation under cyclic loading conditions. This work has largely been based on the application of the Paris-Erdogan law (6), which relates the rate of crack growth to the range of stress intensity factors. Some studies have modeled fatigue crack growth by considering the cohesive stresses in the fracture process zone (7). However, there is a relative lack of studies focused on compressive fatigue, especially regarding the size effect on fatigue life in concrete cubes. While studies on prismatic specimens under axial load (8) and cyclic tests on cylinders of varying diameters and slenderness ratios (9) have provided valuable insights, much remains to be understood about how concrete behaves under compressive fatigue loading.

The incorporation of fibers into concrete as a distributed reinforcement leads to a more ductile material once the concrete matrix breaks, which is manifested in bending (10), but also in tension (11) and compression (12), and can also lead to modifying the effect of

the size (13). Fiber reinforced concrete already plays a significant role in modern construction applications due to its enhanced ductility and post-cracking tensile strength, which makes it more enduring to fatigue compared to plain concrete (14). Research shows that fiber reinforcement generally improves fatigue resistance, though the fibers' influence under compressive stress is more limited, as they can sometimes act as crack initiation points (14–16). Fiber reinforced concrete demonstrates more uniform fatigue behavior across different loading frequencies, with steel fibers, in particular, helping to mitigate the detrimental effects of low-frequency loading (17). However, it has been observed that there is an optimal fiber content, beyond which the fatigue life of the material decreases (14). Additionally, few studies have examined the size effect specifically in fiber reinforced concrete. Some research, such as (18), suggests that fiber addition shifts the brittle-to-ductile transition in bending tests, while other studies have found that increasing both matrix strength and fiber content reduces the size effect in compressive fatigue tests (19).

Parallel to the study of size effects on fatigue, there is growing interest in the phenomenon of autogenous self-healing in concrete under fatigue conditions. Contrary to the traditional view that cyclic loading degrades material properties over time, by the late 1900s and early 2000s some research showed that concrete can exhibit strength increases after undergoing fatigue loading. For example, Nelson *et al.* (20) observed a remarkable 39% strength increase in runout specimens, and Taliercio and Gobbi (21) reported strength gains between 6% and 33% due to lateral confinement in axially fatigued concrete. Taher and Fawzy (8) extended these findings, demonstrating that normal-strength concrete can exhibit strength gains of 15% to 57% after a limited number of fatigue cycles. Cachim *et al.* (22) confirmed similar results for both plain and fiber reinforced concrete, noting improvements up to 16%. More recent studies, including those by Malek *et al.* (23), Qiu *et al.* (24), and Garijo *et al.* (25), have further corroborated these observations, with strength increases as high as 42%.

The underlying mechanism for this strength increase is thought to be autogenous self-healing, where microcracks generated by cyclic loading allow occluded water to penetrate the material, rehydrating dormant cement particles and sealing the cracks (25–28). Various mechanisms have been proposed for this self-healing process, including calcium carbonate precipitation, the rehydration of unhydrated cement particles, the obstruction of cracks by impurities, and the swelling of the hydrated cement matrix (29–34). Some researchers emphasize the role of calcium carbonate precipitation (33, 35), while others highlight

the importance of ongoing hydration reactions (36). The ability of concrete to self-heal is dependent on several factors, including the availability of moisture, the size of the cracks, and the use of fibers to control crack width and propagate stress in a more distributed manner (29, 36–38).

In addition, advances in nanotechnology have provided opportunities to enhance the autogenous self-healing capabilities of concrete by incorporating nanomaterials that act as nucleation sites for the formation of new hydration products (39). This phenomenon has also been observed in ultra-high-performance concretes, where large amounts of cementitious material remain unhydrated. When exposed to moderately elevated temperatures, such as those exceeding 200°C, these materials exhibit strength increases due to the activation of dormant hydration processes (40).

Given the importance of both the size effect and autogenous self-healing in understanding the fatigue behavior of steel fiber reinforced concrete, we planned to investigate these two phenomena in detail. We focused on the compressive fatigue life of cubic and cylindrical specimens of varying sizes and explore how cyclic loading-induced microcracks contribute to the autogenous self-healing process. The research has already led to some publications that are summarized in this paper. The first two of them dealt with the size effect of cubes and cylinders of a single steel fiber reinforced concrete in fatigue (26, 27). Their results manifested that there could be autogenous self-healing in the specimens that endured most, which made us prepare another research that eventually demonstrated the production of new hydration products

due to fatigue (28). In this paper, we want to give a comprehensive view of these coupled phenomena. By combining probabilistic analysis of fatigue life with detailed microstructural and fracture assessments, we seek to provide a comprehensive understanding of how size and self-healing influence the mechanical behavior of concrete under fatigue conditions.

We also aim to familiarize the reader with the concept of steel fiber reinforced concrete (SFRC) fatigue in compression. This understanding is crucial for recognizing the significance of size effect and the initiation of autogenous self-healing caused by compressive fatigue loads. To achieve this, we delve into the study of concrete fatigue in compression, drawing from our own scientific research. This research has been driven by collaboration with industrial partners interested in investigating the fatigue of structural components, such as pylons for wind turbines (see Figure 1a), slabs for high-speed train tracks (Figure 1b) (41, 42), and encased composite beams with steel fiber reinforced concrete (Figure 1c) (43).

We will first discuss the phenomenology of fatigue of steel fiber reinforced concrete in compression. This will include subsections covering basic aspects of representing fatigue results (Subsection 2.1), as well as the effects of experimental scatter (2.2), frequency (2.3), fiber content (2.4), and load eccentricity (2.5). Section 3 will focus on the impact of size on the compressive fatigue of the material, while Section 4 will deal with autogenous self-healing due to fatigue (Section 4). It follows a discussion on the principal effects influencing autogenous self-healing, namely mineral additions (Subsection 5.1), carbonation (5.2), steel fiber reinforcement (5.3), size effect (5.4), and

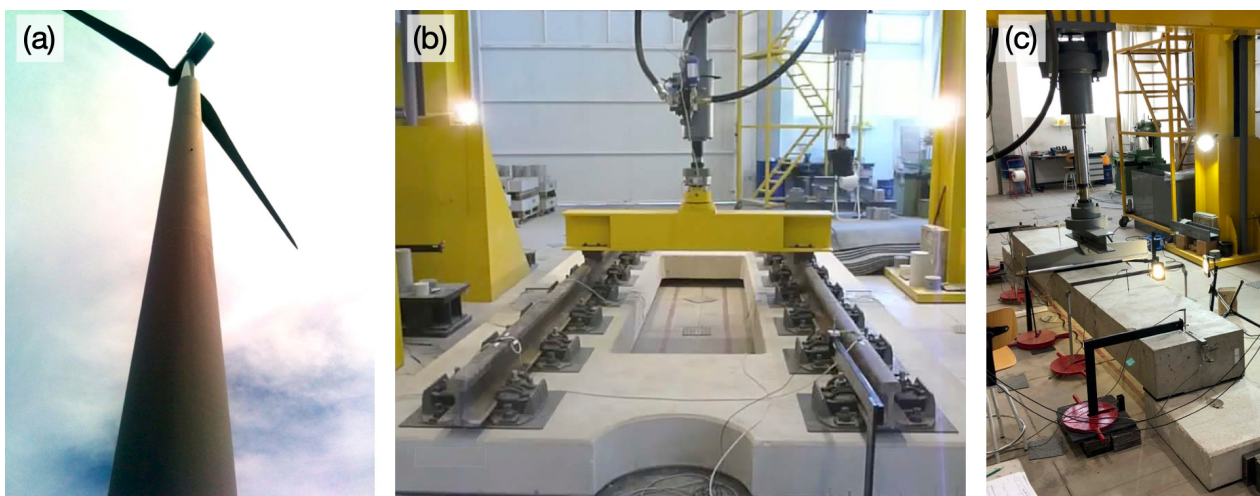


FIGURE 1. (a) SFRC-tower supporting a wind turbine. Fatigue tests of: (b) a reinforced concrete slab for high-speed ballastless tracks (41, 42), and (c) an encased composite beam with steel fiber reinforced concrete (43), both made in the Materials and Structures Laboratory at UCLM.

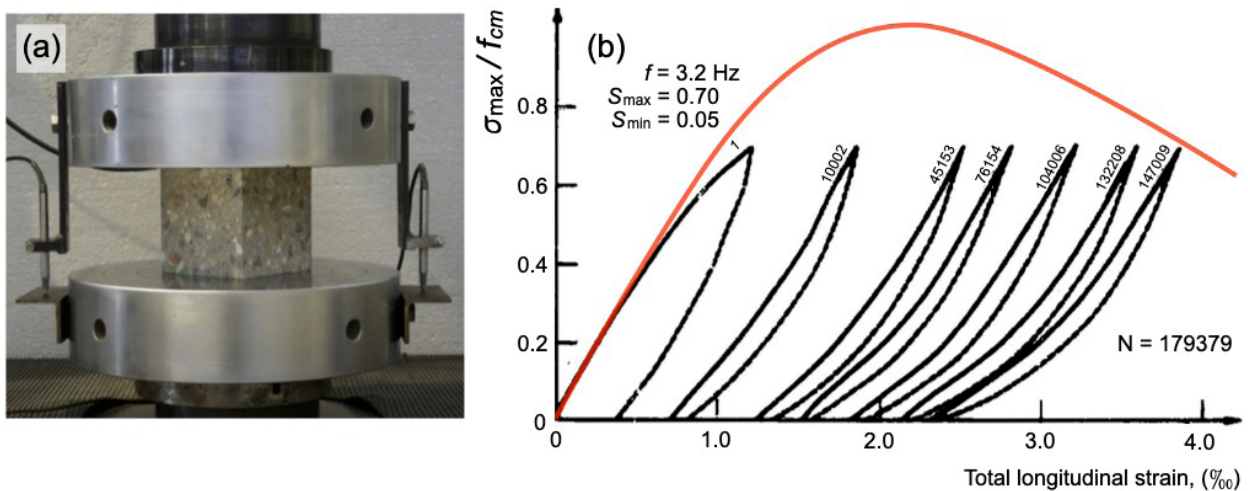


FIGURE 2. (a) Concrete cube tested in compressive fatigue and (b) stress-strain cycles in compression plotted with the stress-strain monotonic curve of the same material (adapted from Figure 6.4, P. Jinawath PhD Thesis Report, University of Leeds, 1974 (44), & Figure 8.23 in (45)).

time (5.5). Lastly, we will draw conclusions emphasizing the importance of taking these phenomena into account.

2. FATIGUE PHENOMENOLOGY IN CEMENTITIOUS MATERIALS

Cyclic loading in concrete, whether compressive or tensile, causes the material to experience strain increments with each cycle. Figure 2a illustrates a typical setup of a compressive fatigue test on a concrete cube, whereas Figure 2b plots some compressive load-strain loops in a specimen that has been subjected to cycles running from 5% to 70% of its compressive strength. They correspond to a $76 \times 76 \times 302 \text{ mm}^3$ prism of a 36 MPa concrete tested by Jinawath (44). The compression loops initially exhibit a convex shape during loading and a concave shape during unloading, but soon they feature a concave loading branch. The secant modulus of elasticity decreases as the number of cycles increases, as illustrated in Figure 2b. The strain increase is rapid during the first few cycles, then levels off and becomes linear with the number of cycles during a second phase, and eventually grows rapidly again before failure, as depicted by the strain-number of cycles curve in Figure 3. This curve is often referred to as the “cyclic creep curve” because it resembles the deformation caused by a sustained load on the material. The average of the cyclic loading affects the specimen, and the resulting deformation somehow responds to this mean load.

The stress-strain loops show that there are internal surfaces and microcracks present in the concrete,

caused by the loads, which then grow. These internal surfaces come into contact again when the test piece is compressed anew in the following cycles, leading to overall hardening that is reflected in the concavity of the load branch in compression (interestingly, no hardening is observed in tension because the surfaces do not come into contact (46)). The area enclosed in the loops represents energy dissipation due to the generation and propagation of microcracks, and friction between internal surfaces. Failure occurs when the concrete reaches a critical deformation that it can no longer withstand. For example, in Figure 2b, the critical elongation of the last cycle approximately coincides with the elongation recorded in the static test for that level of compression, schematically represented by the solid red curve. This observation suggests that the static resistance curve can be considered as a failure curve of the fatigue loops, like an envelope of the cyclic loops. Indeed, it is usually

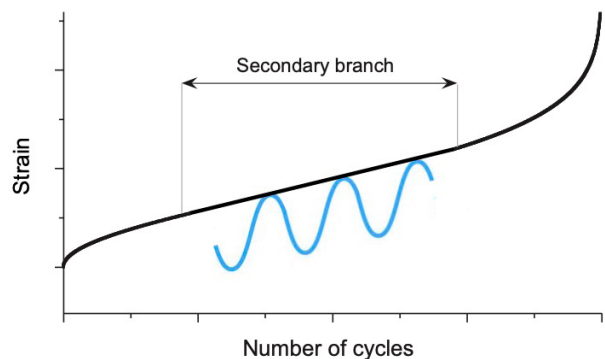


FIGURE 3. Cyclic creep curve in cementitious materials.

considered that fatigue failure takes place once the loops reach the quasi-static envelope (47–49). It is confirmed that the deformations at the end of the second phase are similar to those of the envelope, while the critical deformations exceed those obtained in static tests (48). However, due to the scatter of the post-peak part of the monotonic quasi-static curve, especially in concrete with fibers, and its dependence on the geometry of the specimen, this observation cannot be profitably used for predicting accurately the fatigue life (12, 26, 50, 51).

2.1. Stress/strain vs. number of cycles curves in concrete

Figure 4 illustrates the relationship between the logarithm of the secondary strain rate per cycle (which corresponds to the constant strain rate during the second stage of the cyclic creep curve, as shown in Figure 3) and the logarithm of the number of cycles to failure for three different types of concrete with the same matrix (17). The types are as follows: C1 is plain concrete, with a compressive strength of 56 MPa at 28 days; C2 is polypropylene fiber-reinforced concrete, with a compressive strength of 66 MPa and a fiber volume of 0.56%; and C3 is steel fiber-reinforced concrete, with a compressive strength of 67 MPa and a fiber volume of 0.64%.

Tests were conducted on 100 mm cubes at four different frequencies: 4 Hz, 1 Hz, 1/4 Hz, and 1/16 Hz. All data points generally align along a straight line, a trend first noted by Sparks and Menzies (52) for plain concrete. Medeiros *et al.* (17) further demonstrated that this relationship holds true regardless of the type of fiber or the testing frequency. The linear relationship can be expressed as:

$$\log \frac{\dot{\epsilon}}{f} = m + s \log N \quad [1]$$

where $\dot{\epsilon}/f$ is the secondary strain rate per cycle, f is the frequency, and N is the number of cycles endured before failure (note that $\dot{\epsilon}/f = d\epsilon/dn$, where n represents the cycle number, not the cycle at failure).

This feature of cyclic creep curves enables the derivation of a strain-based failure criterion. Poveda *et al.* (14) extended the Sparks and Menzies’ law by integrating it to yield a failure criterion expressed as:

$$\epsilon_c = \epsilon_{max} + 10^m N^{s+1} \quad [2]$$

where ϵ_c is the critical strain at failure and ϵ_{max} is the maximum strain recorded in the first cycle. The red curve in Figure 5 represents this criterion on a strain vs. number of cycles plot. Failure of a specimen oc-

curs when the cyclic creep curve intersects this failure curve, as indicated by the black dots in Figure 5.

While strain-based failure criteria offer a convenient method for assessing fatigue behavior, the fatigue strength of concrete is often represented by $S-N$ curves. In these curves, S represents the normalized stress ($S = \sigma/f_c$) and N is the number of cycles to failure, typically shown on a logarithmic scale. For instance, the $S-N$ curves proposed in the 2010 Model Code and developed by Lohaus *et al.* (53) (see Figure 6) illustrate the relationship between maximum stress and N , with the minimum stress as a parameter. These curves are generally considered applicable to all types of concrete, as the influence of composition on fatigue behavior is relatively minor.

A distinction is often made between low-cycle and high-cycle fatigue. Low-cycle fatigue results from a small number of cycles at high stress levels, such as those during an earthquake, whereas high-cycle fatigue occurs over the structure’s service life at lower stress levels. However, both fatigue types are driven by the same damage mechanisms, making the distinction largely formal. According to CEB Committee 188 (54), the boundary between low-cycle and high-cycle fatigue lies between 10^3 and 10^4 cycles, but no clear discontinuity is observed in the $S-N$ curves (Figure 6b).

Unlike metals, concrete appears to lack an endurance limit, meaning no stress threshold guarantees infinite fatigue life. Tests beyond 10^7 cycles are uncommon, yet the Model Code curves (Figure 6b) extend up to 10^{20} cycles. Reaching this extreme number of cycles at a frequency of 1 Hz would take approximately 230 times the time since the Big Bang—about 13.8 billion years, which gives an idea of the absolute nonsense of extrapolating results in the logarithmic scale.

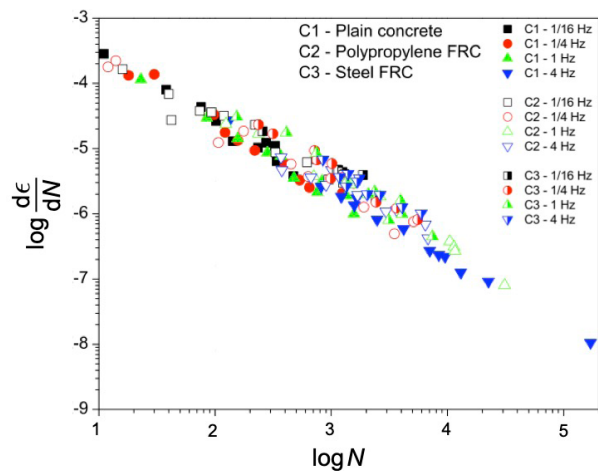


FIGURE 4. Logarithm of the number of cycles to failure versus the logarithm of the secondary strain rate for three concretes with a shared matrix (17).

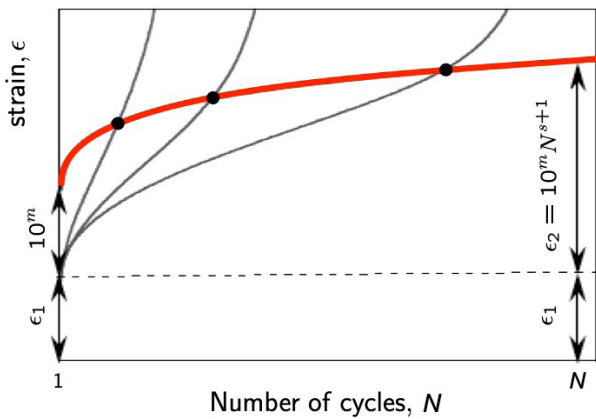


FIGURE 5. Graphical representation of the failure criterion based on the Sparks & Menzies law by Poveda *et al.* (14).

Concrete’s fatigue life is highly sensitive to both the stress level and the loading range, defined by the difference between maximum and minimum stress ($\Delta\sigma = \sigma_{\max} - \sigma_{\min}$), or by the stress ratio $R = \sigma_{\min} / \sigma_{\max}$. A smaller stress range or higher stress ratio allows the concrete to withstand a greater maximum cyclic load. This relationship is shown in Figure 6b, where higher minimum stresses correspond to higher maximum stresses in cyclic loading.

2.2. Experimental scatter

It is important to understand that concrete fatigue can vary significantly, meaning that a single average *S-N* curve may not fully represent all fatigue behaviors. Figure 7 illustrates this by displaying the proba-

bility of failure versus the number of cycles for almost 100 identical compression fatigue tests conducted by Ortega *et al.* (56). The compressive strength of the SFRC was 58.9 MPa, and it was reinforced with 13 mm straight steel fibers at a 0.2% volumetric ratio. The results were analyzed using a two-parameter Weibull function. By randomly selecting test groups and plotting their failure probability functions, we can estimate the range of error associated with different sample sizes.

In Figure 7, the shaded area represents the range covered by random groups of 25 tests. It required half a million random groups to stabilize this band and have it aligned with the overall distribution obtained from all tests, represented by the thick black line, which is considered the correct distribution. From this, we can derive the probability density function for various failure probabilities and calculate confidence margins. For example, the green curve shows the density function for a 40% failure probability, while the dashed blue line indicates the 95% confidence margin. This means there is a 95% likelihood that the distribution function of a random group of 25 tests will fall to the left of this curve.

The right plot in Figure 7 presents error curves for different sample sizes, enabling us to determine the associated error for each group size. For instance, the relative error for a group of 15 fatigue tests (orange error curve) is 5.7% at a 50% failure probability, rising to 10.5% for groups of 5 tests (red curve), and decreasing to 4.1% for groups of 25 tests (blue curve). If the failure probability is 10%, the relative errors increase to 22.2%, 10.9%, and 7.5% for groups of 5, 15, and 25 specimens, respectively.

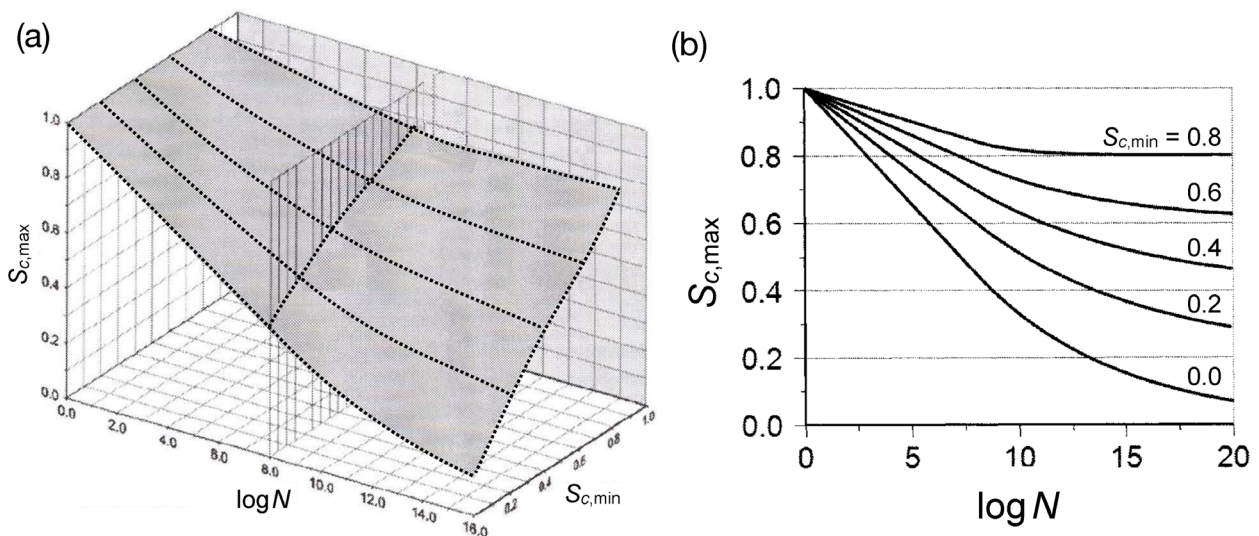


FIGURE 6. *S-N* curves for concrete according to the Model Code 2010 (55): (a) 3D representation from the model by Lohaus, Oneschkow, and Wefer (53), and (b) 2D plot included in the standard.

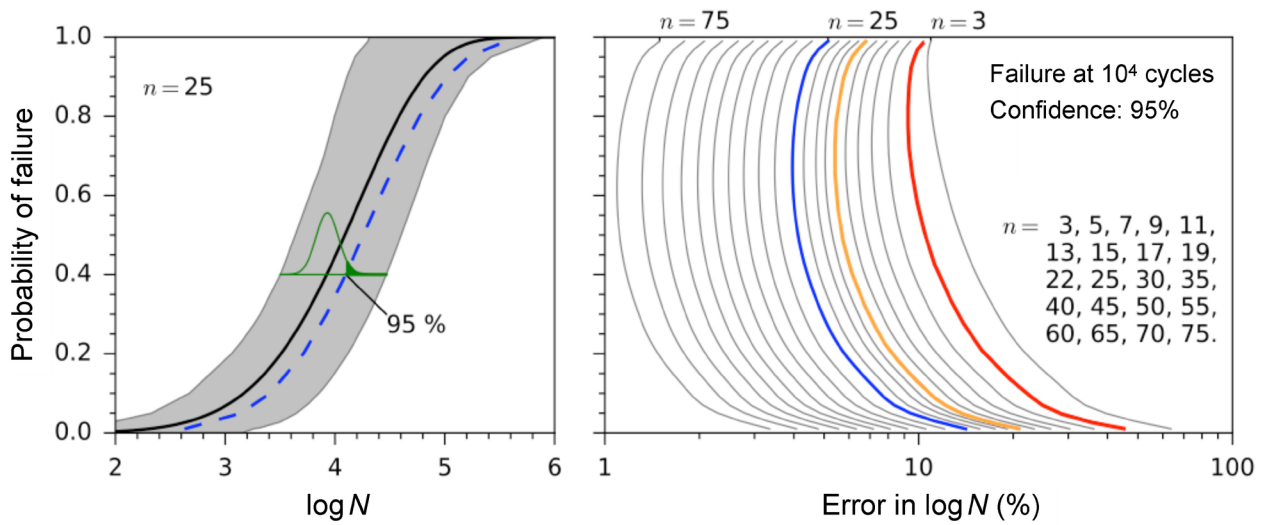


FIGURE 7. Effect of sample size (n) on the measurement of fatigue life. The shaded band represents the variability in failure probability for random groups of 25 tests. The right plot shows relative error curves for different sample sizes (56).

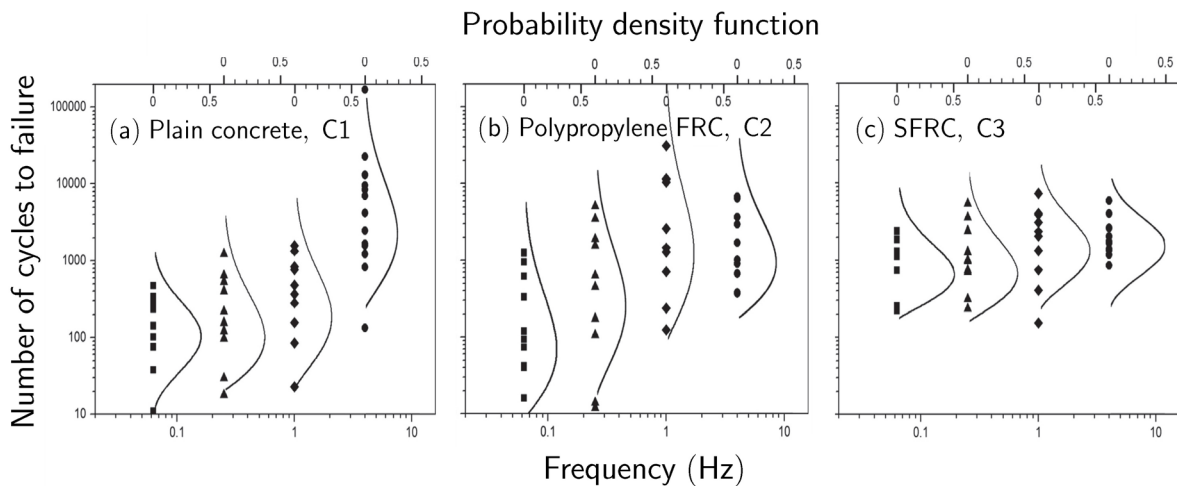


FIGURE 8. Effect of frequency on fatigue life for three concretes with the same matrix (17): (a) plain concrete (C1), (b) polypropylene fiber reinforced concrete (C2), and (c) steel fiber reinforced concrete (C3).

Even with large sample sizes, there is considerable variability in failure probabilities. In this example (Figure 7), the average fatigue life is approximately 10700 cycles, but at a 10% failure probability, the fatigue life drops to just 1500 cycles. $S-N$ curves are typically constructed using the average values of the failure distribution for each load case, necessitating a statistical approach to ensure adequate safety levels.

2.3. Effect of frequency

The frequency of cyclic loading significantly affects fatigue life, especially at low frequencies (1 Hz and below) and high peak stresses (above 75% of stat-

ic strength). Figure 8 presents fatigue life results at varying frequencies (4, 1, 1/4, and 1/16 Hz) for compression tests with a peak load of 85% of the static strength (79 MPa for the C1 concrete, tested when it was approximately one year old) and a stress ratio of 0.3 (17). A notable drop in fatigue life occurs when shifting from 4 Hz to 1 Hz, where $\log N$ decreases from 4.3 to 2.8, indicating a reduction in fatigue life by more than an order of magnitude. This reduction results from lower strain rates at reduced frequencies, which diminish static strength. Additionally, the interaction between the detrimental effects of compressive cycles and the beneficial self-healing due to fatigue may play a role in this behavior (discussed later in Section 5).

This sensitivity to frequency is particularly relevant for structures like wind towers, which experience low oscillation frequencies. To improve fatigue life in such applications, reinforcing concrete with steel fibers is advisable, as they help extend fatigue life. For instance, concrete C3 (steel fiber reinforced) in Figure 8 shows consistent performance across all studied frequencies, unlike C2 (polypropylene fiber reinforced), which is more frequency sensitive.

2.4. Effect of fiber content

We investigated the effect of fiber content on the mechanical behavior of steel-fiber reinforced concrete (SFRC) under low-cycle fatigue (14). Five self-compacting concrete mixtures were designed with fiber contents ranging from 0 to 0.8% by volume. All mixtures shared the same concrete matrix, ensuring flowability and fiber-matrix adhesion. The base concrete had a compressive strength of 33.4 MPa. The steel fibers used were hook-ended, 35 mm in length, and 0.55 mm in diameter. The specimens were 100 mm cubes.

In terms of static behavior, the fibers did not significantly enhance compressive strength. However, the presence of fibers resulted in a more gradual post-peak softening after maximum load. Regarding flexural behavior, increasing fiber content improved post-peak performance, though certain fiber amounts produced similar residual tensile strength. For example, concrete with 0.6% fiber content exhibited post-peak behavior similar to that with 0.4%.

The addition of steel fibers markedly improved compressive fatigue performance, as fatigue life in-

creased with fiber content (see Figure 9a). Low fiber contents did not substantially improve fatigue properties compared to plain concrete. However, intermediate fiber contents—from 0.4% to 0.6%—extended fatigue life up to five times longer than that of plain concrete (equivalent to a 31% increase in the logarithmic average of resisted cycles). The optimal fiber dosage was found to be 45 kg/m³ in this particular study. Interestingly, higher fiber contents reduced fatigue life, likely due to increased matrix imperfections and pore formation, which promote crack initiation.

Notably, the Sparks and Menzies' plot of secondary strain rate versus fatigue life showed a consistent linear relationship (Figure 9b), confirming that this relationship is independent of fiber content and primarily depends on the base concrete.

The improvement in fatigue life with fiber content may be explained by the interplay between microcrack propagation and autogenous self-healing due to fatigue, which will be discussed further in Section 5.

2.5. Effect of load eccentricity

We also examined how load positioning uncertainty affects the fatigue life and result variability of SFRC (57), a factor often blamed on compressive strength scatter (22, 45). While inhomogeneity at the mesoscale undoubtedly contributes to scatter, there may be experimental factors influencing fatigue life as well.

To reduce unintended loading eccentricity, we developed an individualized ball-and-socket joint (i-BSJ)

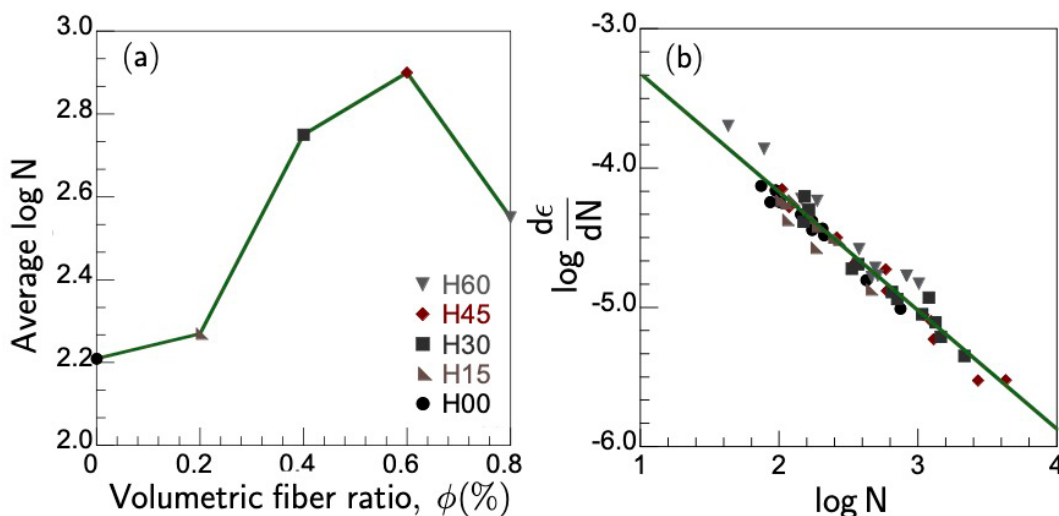


FIGURE 9. Effect of fiber content on fatigue life of SFRC (14): (a) Fatigue life as a function of fiber dosage; (b) Secondary strain rate vs. fatigue life following Sparks and Menzies' model.

(see Figure 10a). Two types of tests were conducted: first, we used an instrumented aluminum cube to measure eccentricity under two conditions—using the i-BSJ and without it. Second, two series of 15 monotonic compressive tests and two series of 15 cyclic compressive tests were performed on 40 mm SFRC cubes (using 15 kg/m³ of straight, 13 mm long, and 0.20 mm in diameter fibers), again with and without the i-BSJ.

The results revealed that while average eccentricity values remained similar, their standard deviation was reduced by an order of magnitude when using the i-BSJ. Figure 10b illustrates the two-dimensional probability distribution of load position. Without the i-BSJ, load eccentricity had wider variation (grey-shaded area in Figure 10b), whereas with the i-BSJ, it was significantly more concentrated (red-shaded area). Thus, while some variability remained due to equipment tolerances and specimen geometry, the i-BSJ effectively minimized misalignments from manual specimen centering and other geometrical factors.

In addition, when the i-BSJ was used in the SFRC cube tests, the average compressive strength increased by 10% (from 53.6 MPa to 58.9 MPa). The average fatigue life also saw a significant increase, multiplying by six in the second series (refer to the red curve in Figure 10c). Furthermore, the standard deviation of fatigue life decreased, as indicated by the steeper slope of the red curve in Figure 10c. These results show that undesired loading eccentricity reduces fatigue life and increases result variation, beyond what can be explained by variations in compressive strength alone (22, 45).

In conclusion, when testing specimens in compressive fatigue, it is highly recommended to use an i-BSJ for minimizing the uncertainties caused by manual centering misalignments in both monotonic and cyclic compressive tests.

TABLE 1. SFRC dosage (size-effect study).

Component	Content (kg/m ³)
Cement CEM II/B-L 32.5 N	286
Limestone filler	195
Water	202
Air reducer (MasterCast 212)	1
Superplasticizer (MasterEase 5025)	2.86
Sand 0.5 mm (feldspathic)	921
Coarse agg. 4–8 mm (siliceous, crushed)	712
Steel fiber OL 13/.20	23.55

3. SIZE EFFECT IN FATIGUE OF SFRC

As anticipated in the introduction, we also studied the size effect on fatigue in self-compacting steel-fiber reinforced concrete specimens. Cubes of three sizes (40 mm, 80 mm, and 150 mm edge lengths) (26) and cylinders of three heights (75 mm, 200 mm, and 300 mm) were tested, with slenderness 2 for the cylinders (Figure 11) (27). All the specimens were made from the same self-compacting steel fiber reinforced concrete. The composition is detailed in Table 1. The fiber content was 0.3% by volume, and the type used was straight fibers, specifically Dramix OL 13/20 from Bekaert, measuring 13 mm in length with an aspect ratio of 65. This length was selected to ensure that the fibers remained sufficiently short relative to the smallest specimen size, maintaining the homogeneity of mechanical properties throughout the material.

Cubes and cylinders were stored in a humid chamber maintained at 20°C and 97% relative humidity for at least one year after demolding. The mean compressive strength of the hardened concrete was measured at 28 days. The results showed an aver-

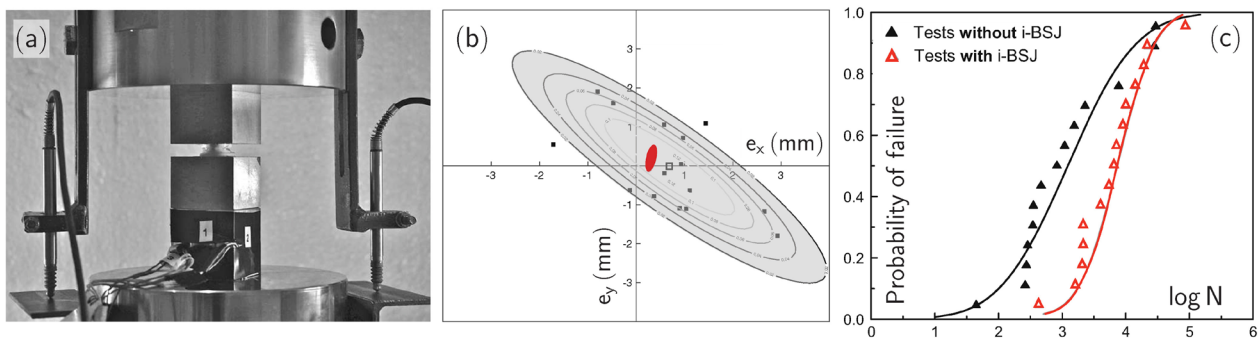


FIGURE 10. Impact of eccentricity on fatigue life (57): (a) 40-mm SFRC cube tested with an individualized ball-and-socket joint (i-BSJ); (b) Probability density function for load eccentricity in two test series (90% of results without i-BSJ fall within the grey area, while 90% of results with i-BSJ fall within the red area); (c) Fatigue results for identical SFRC specimens tested with and without the i-BSJ.

age of 26.4 MPa from cylinders with a diameter of 75 mm and a height of 150 mm, and 28.2 MPa from cubes with an edge length of 100 mm. Additionally, the compressive strength of cylinders with the same dimensions was tested at 56 days and yielded an average of 30.6 MPa. The properties exhibited a high degree of homogeneity, as indicated by their small standard deviations (26, 27).

For each size, 10 quasi-static tests were conducted right before fatigue testing to determine their reference compressive strength, followed by 15 fatigue tests with cyclic loads ranging from 0.20 to 0.85 of the compressive strength. As strain along the loading direction in cubes is not uniform due to the confining effect of friction in contact with the platens, we preferred taking the average strain, i.e. total deformation over the cube's edge length, measured as the average between the readings of two LVDTs as a representative value. As for the cylinders, they have a slenderness of 2, so the influence of the contact with the platens in the central section is negligible, and thus we took the strain in the central point of the height, actually the average between the recordings of three strain gauges at 120°.

A key strength of this methodology lies in the use of diverse equipment to control tests and assess internal changes, including ball-and-socket joints to minimize misalignment and devices like a computed tomography scanner and mercury porosimeter to analyze internal structure and failure modes. Additionally, the number of specimens allowed for a more accurate representation of the probabilistic nature of both quasi-static and fatigue results.

For cubes, the reference compressive strength was consistent across all sizes, with means of 30.5 MPa, 30.6 MPa, and 30.7 MPa for small, intermediate, and large cubes, respectively. This lack of size effect reflects the material's high post-peak ductility from fiber reinforcement, leading to a failure closer to plastic behavior than quasi-brittle. This may change for larger sizes (1, 2, 13). In contrast, the quasi-static reference compressive strength of cylinders displayed a slight inverse size effect: the mean compressive strength increased from 26.3 MPa for small cylinders to 32.5 MPa for large ones. This was attributed to a reduction in porosity near the cylinder surfaces as size increased, as detected by the computed tomography study (27, 58). The inverse size effect impacts fatigue behavior: smaller cylinders experience lower maximum and minimum loads, contributing to longer fatigue lives, while larger cylinders benefit from higher static strength. However, other size-dependent factors may counteract these effects.

In terms of fatigue life, 80 mm and 150 mm cubes showed similar Weibull distributions, while 40 mm

cubes exhibited much higher scatter, spanning over two orders of magnitude at 50% failure probability (Figure 12). Many smaller cubes survived longer cycles, indicating an autogenous self-healing effect. Post-fatigue monotonic tests on run-out cubes revealed a 42% strength increase compared to initial values (43.2 MPa compared with the initial 30.5 MPa). This could be due to cyclic loading inducing microcracks, allowing water to react with unhydrated cement and thus improving strength. Cylinders followed a similar pattern: small cylinders had longer lives compared to larger ones, suggesting self-healing, though not as pronounced as with cubes. No runouts occurred in the cylinder tests.

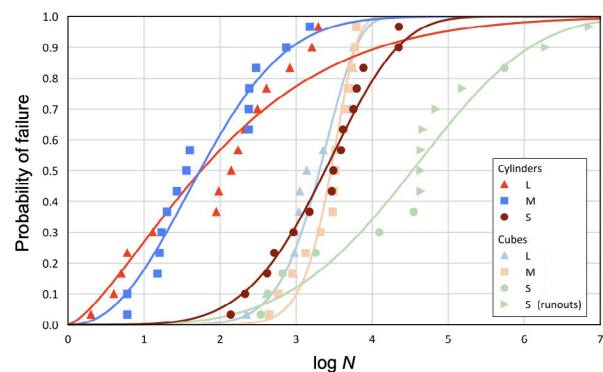


FIGURE 12. Plot representing the cumulative probability of failure vs. fatigue life of cubes and cylinders of three sizes made of the same SFRC (26, 27).

It is important to emphasize that all the cylinder and cube specimens, which results are shown in Figure 12 covering seven orders of magnitude in N , were

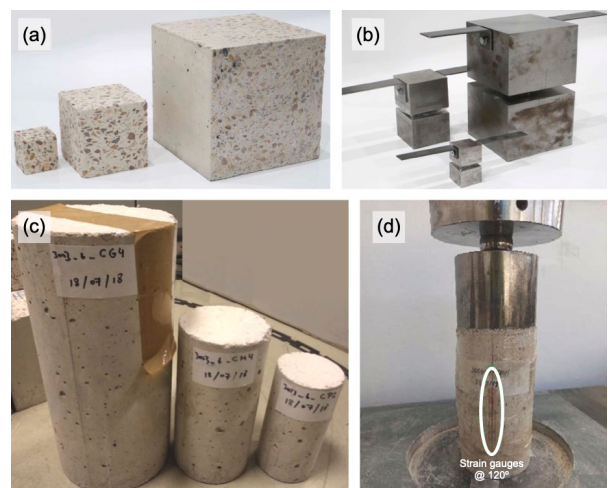


FIGURE 11. (a) SFRC cubes of three sizes: 40 mm, 80 mm, and 150 mm; (b) individualized ball and socket joints for the three cubes (26); (c) SFRC cylinders of three heights: 150 mm, 200 mm, and 300 mm; (d) fatigue test of one of the medium cylinders (27).

made of the same material, and all tests were conducted at 20% to 85% of the reference compressive strength of the respective series. The findings indicate that the size of the specimen has a significant impact on fatigue life. Additionally, the specimen's shape has a considerable effect on fatigue behavior, with cylinders being more conservative than cubes. We believe that cubes provide more confinement to the material, facilitating the extension of micro-damage in a stable manner and allowing self-healing to happen in all these damaged regions, as discussed in the next section. These results highlight the significant size effect in fatigue testing, cautioning against using small specimen data to characterize structural element behavior.

4. AUTOGENOUS SELF-HEALING DUE TO FATIGUE

During our study of fatigue aspects of SFRC, we observed significant improvement in the material after compressive fatigue loading. However, there were various hypotheses to explain this behavior that lacked sufficient evidence. To address this, we initiated further research to identify the changes in the material's microstructure caused by compressive fatigue and to determine if there is an increase in the production of hydrated compounds due to the fatigue mechanical actions.

As we had found that cubes, not cylinders, experienced runouts (see previous section), we suspected that the confinement by friction against the platens

was causing extensive microdamage due to fatigue, which we believe is associated with the autogenous self-healing phenomenon. Cylinders with a slenderness of 2 have less volume affected by friction with the platens. So, microdamage extension is smaller than in cubes, making them less likely to develop autogenous self-healing. Note that this does not mean cylinders do not experience self-healing since small cylinders endure longer than taller ones, but it is less noticeable than in cubes. Thus, we used only cubes for our new experimental campaign, subjecting specimens to programmed fatigue loading.

For this research on autogenous self-healing induced by fatigue, we collaborated with experts in the chemistry of cement and concrete at the Institute for Construction Sciences "Eduardo Torroja". They designed and fabricated the SFRC (see the composition in Table 2) and conducted and analyzed physical tests that complemented our fatigue tests. The result was a publication on the autogenous self-healing of SFRC (28), which we will describe in this section.

4.1. Mechanical tests

4.1.1. Compressive tests

Compressive tests were conducted on six 100 mm cubes, all made with the corresponding ball-and-socket joint, to determine their reference compressive strength just before the beginning of fatigue tests, when the SFRC was four months old. The cubes were

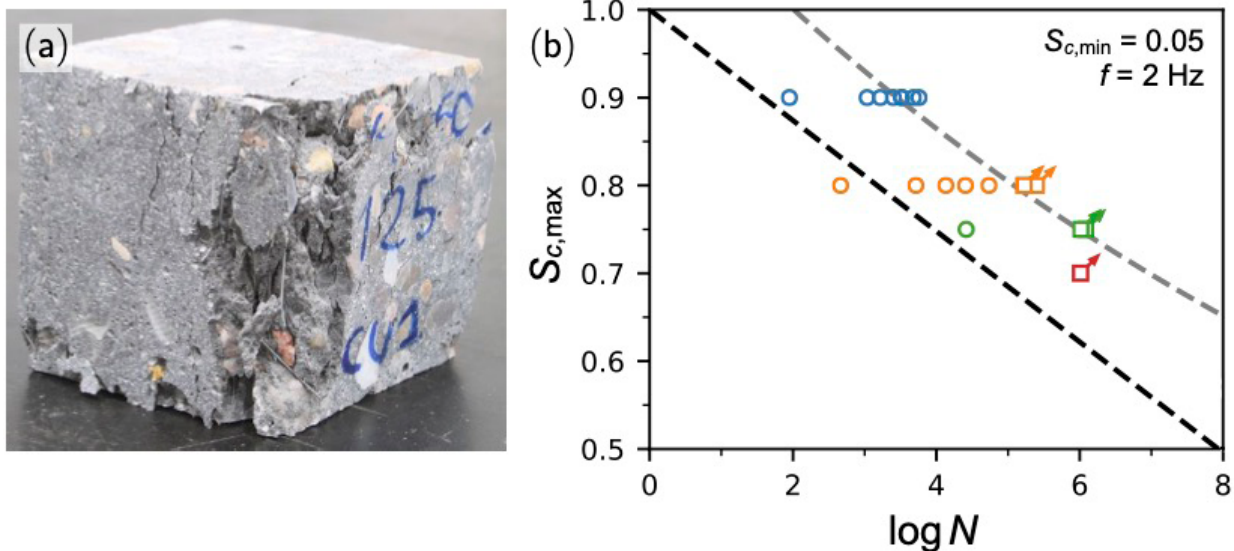


FIGURE 13. (a) 80 mm cube of a series of high strength SFRC tested monotonically; (b) fatigue results of this material for four stress levels (28); the dashed black straight line is the $S-N$ curve given by the Model Code 2010 (54) and the dashed grey line is given by the model of Saucedo *et al.* (59) for a probability of failure of 50%.

kept in a humid chamber until then. In Figure 13a, one of the cubes is shown immediately after testing. The average value obtained was 77.6 MPa, with a small standard deviation of 2.4 MPa, resulting in a coefficient of variation of only 3%. This indicates that the mechanical behavior of this concrete for this specimen size is very consistent. Using the ball-and-socket joint contributed to this result by eliminating the source of scatter caused by load eccentricity, which is unrelated to the material (as shown in Subsection 2.5).

TABLE 2. SFRC dosage (autogenous self-healing study).

Component	Content (kg/m ³)
Cement CEM I 52.5 N	465
Silica fume	46
Limestone filler	74
Water	181
Superplasticizer (MasterEase 3690)	7.3
Sand 4 mm (siliceous)	811
Coarse agg. 4–12 mm (siliceous, crushed)	803
Steel fiber 4D 65/35 BG	60

4.1.2. Fatigue tests

After determining the mean strength, we carried out fatigue tests at four stress ranges, all starting from minimum stress of 5% the minimum reference strength to 70%, 75%, 80%, and 90% the reference strength. The number of tests for each stress level was determined based on the expected chances of specimen failure. In Figure 13b, the S - N curves show the relationship between the maximum stress level $S_{c,max} = \sigma_{max}/f_c$ and the logarithm of the number of cycles N . As expected, the mean number of cycles and the number of runout specimens increase as the maximum stress decreases. Runout specimens are denoted by markers with an arrow that mainly overlap, as they represent points with similar coordinates (for instance, there were 3 runouts for $S_{c,max} = 0.8$, and 5 for $S_{c,max} = 0.75$, which are almost overlapped in Figure 13b). The distribution of the results is compared with the fatigue life prediction model included in the Model Code 2010 (54) for the minimum stress level used. Most of the points lie to the right of the model, so its prediction can be considered conservative, at least for this type of fiber reinforced concrete.

To accurately describe the material's behavior, the probabilistic model by Saucedo *et al.* (59) has been applied to fit the experimental data. This model incorporates the initial distribution, corresponding to quasi-static tests as the failure limit for one cycle while accounting for the dynamic effects of loading

frequency. Consequently, the extrapolation for $\log N = 0$ exceeds $S_{c,max} = 1$. The fatigue data fitting was performed for $S_{c,max} = 0.9$, a case with no runouts, providing complete statistical information. The model line in Figure 13b represents a 50% failure probability, illustrating the estimated mean behavior for other stress levels, assuming the life estimate given by the Sparks and Menzies' law (52) for the runouts.

4.1.3. Fatigue strain

During each fatigue test, strain evolution relative to the number of loading cycles n was recorded. As illustrated in Figure 3, the strain evolution until failure typically follows three stages: primary strain, characterized by rapid growth in the initial cycle interval; secondary strain, exhibiting uniform and stable behavior for most of the test; and tertiary strain, marked by accelerated strain before failure. The stability and duration of the secondary strain make it representative of the material's fatigue creep behavior. The average slope of this phase, or secondary strain rate per cycle $d\epsilon/dn$, is related to the cycles to failure N . For all failed specimens, the data align along a straight line, confirming Sparks and Menzies' law (52) (see Figure 4). Fitting the strain-based failure model of Eq. 1 to the experimental data yields parameters $s = -1.103$ and $m = -2.466$, with a determination coefficient of 0.984. Previous studies (14, 26, 52) demonstrated this relationship remains constant across variables such as loading frequency (17), specimen size (26, 27), and fiber content (14) for fiber reinforced concrete.

While prior work focused on a single stress range, this study extended the analysis to three stress ranges, considering only fatigue-failed specimens. The results confirm the relationship between dE/dn and N remains constant across stress levels. Higher fatigue loads correspond to higher strain rates and shorter fatigue lives (points shift left), while lower loads result in lower strain rates and longer fatigue lives. However, all points follow the same linear trend, suggesting this relationship is a material property. As mentioned above, for runout specimens, the fatigue life can be estimated from the secondary strain rate given by the second stretch of their cyclic creep curves (14), or also using the master cyclic curve developed by Blasón *et al.* (60, 61).

4.1.4. Compressive strength of runout specimens

Runout specimens were immediately tested under quasi-static conditions until failure after the fatigue tests. Nine runout specimens were tested, yielding a

new mean strength of 95.4 MPa, 23% higher than the original strength. The low standard deviation, with a coefficient of variation around 2%, indicates that the strength increase occurred consistently across all specimens. While strength gain due to aging could be a factor, the specimens were tested at different ages over three months, yet no significant strength evolution was observed. Additionally, the compressive strength of the material at the end of the fatigue tests was checked using the last remaining specimen, yielding compressive strength = 87.8 MPa. Although this single value reflects a 13% natural strength increase due to aging, it is still lower than the strength observed in the fatigue-tested specimens. Thus, a significant part of the strength increase in the runout specimens is likely attributable to the cyclic loading.

The following subsections present analyses of microstructural and compositional changes in concrete subjected to cyclic loads compared to a control specimen.

4.2. Physical tests

Physical tests were performed on one of the runouts and on one intact cube serving as a control specimen. The selected runout corresponds to the sixth specimen from the maximum stress level of 0.75 compressive strength, representing the last fatigue test performed. Both runout and control specimens were preserved under the same conditions. Core samples were taken from them and dried in an oven at 100°C for 24 hours to remove moisture and slow down the hydration process as much as possible. Ideally, the samples should have been immersed in ethanol or propanol to completely stop hydration, but since both samples underwent the same treatment, this fact is not highly relevant when comparing their results to observe the effect of fatigue loads on the self-healing process. After the 24-hour drying period, the samples were analyzed, and physical tests (X-ray diffraction, thermogravimetric analysis, etc.) were performed immediately, with all analyses completed within the following 24 hours.

4.2.1. X-Ray Diffraction (XRD)

The X-ray diffraction (XRD) results for the control and runout samples are presented in Figure 14a. No significant differences were observed between the two samples, either in the types of crystalline hydrates formed or their relative amounts. Therefore, if the self-healing process that occurred during the fatigue tests is associated with the formation of hydrated

phases, it is likely related to the less crystalline ones, primarily calcium-silicate-hydrate (C-S-H) gels.

TABLE 3. Portlandite and bound water measured by DTA/TG (in weight percentage).

Sample	Portlandite	Bound water
Runout	2.0	9.7
Control	2.0	9.4

4.2.2. Thermogravimetric Analysis (TGA) and Differential Thermal Analysis (DTA)

Figure 14b illustrates the endothermic heat flow, while Figure 14c depicts the weight loss of the samples during the decomposition process as the temperature rises. The typical peaks observed in cementitious materials are present: the first peak corresponds primarily to the dehydration of ettringite and calcium silicate hydrate (C-S-H) gels; the second peak is associated with the dehydration of portlandite; and the third peak relates to carbonated phases (62).

Although both concretes show similar results, a key difference arises when comparing hydrate contents from TGA results. The portlandite content is similar in both concretes (Table 3), but the bound water content is higher in the runout sample, indicating an increase in hydrates due to fatigue exposure. This increase could be attributed to further hydration of anhydrous phases or pozzolanic reactions between portlandite and silica fume. Since portlandite content is unchanged, cement hydration seems to be the primary mechanism, although pozzolanic reactions cannot be ruled out.

The additional 3% of hydrates formed in the runout sample, though modest, may contribute to healing microcracks generated during fatigue cycles or at least to a partial self-healing process. Detachment of small particles during fatigue may also fill these microcracks, enhancing compressive strength. However, backscattered scanning electron microscopy (BSEM) evaluations in the next section do not clearly detect such detached particles, though hydrated phases are observed growing within microcracks.

These findings underscore the formation of new C-S-H gel after cyclic compressive loading, crucial for early-age strength gains. Notably, no increase in carbonate phases is observed in the runout sample, suggesting carbonation is not the primary driver of self-healing. However, this does not rule out its occurrence, as discussed in the next section. The movement of free water within the concrete matrix, promoted by cyclic loading, likely facilitates hydrate formation, healing incipient cracks generated by the load.

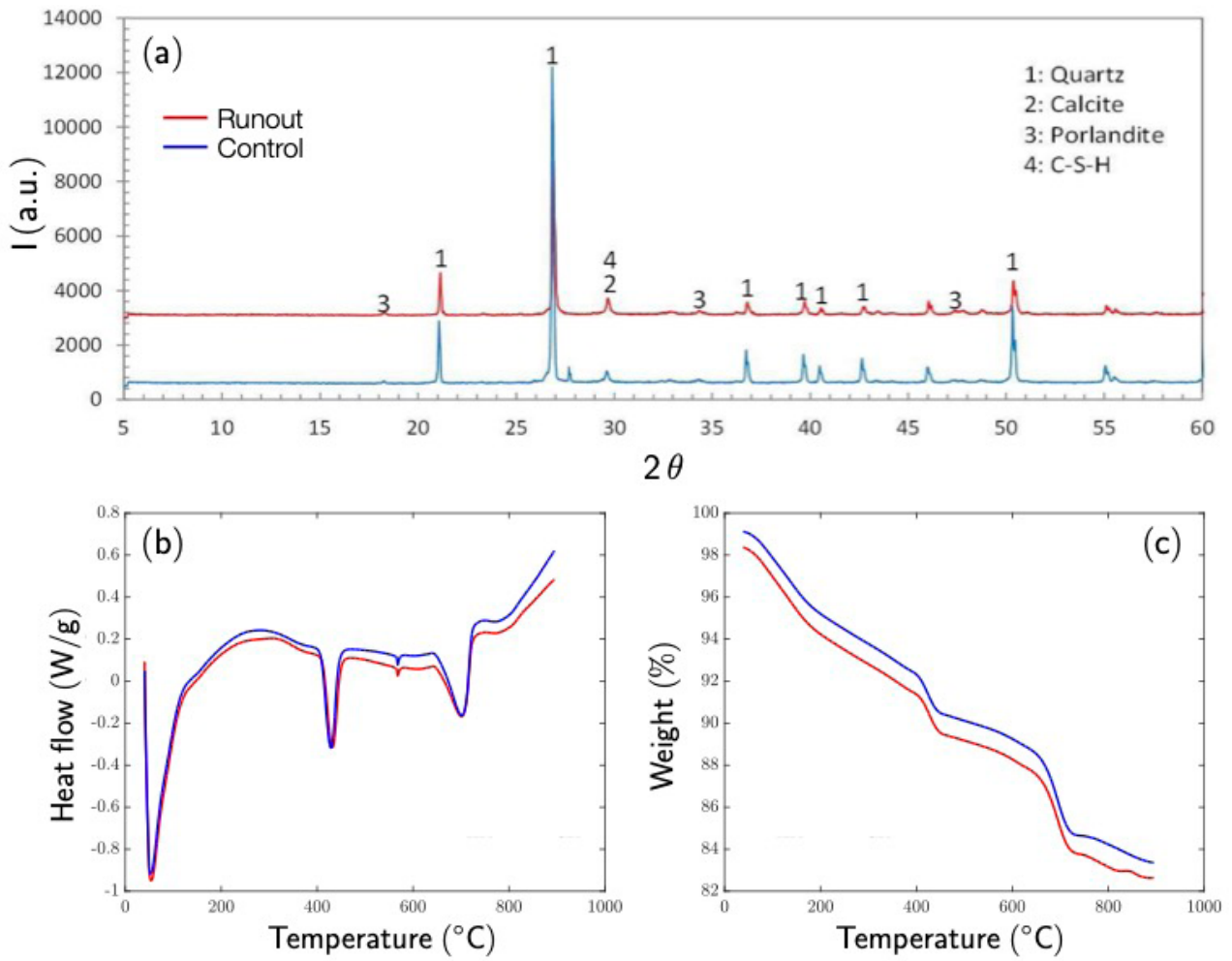


FIGURE 14. Results of physical tests for one the runouts and the non-fatigued control specimen: (a) X-Ray diffractogram; (b) thermogravimetric analysis; and (c) differential thermal analysis (28).

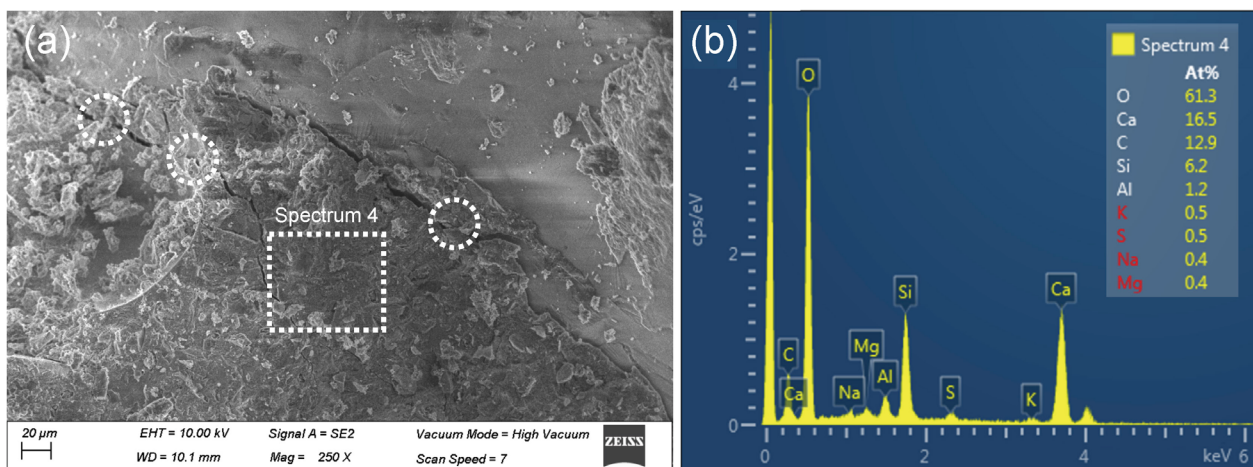


FIGURE 15. (a) BSEM image of a runout specimen, and (b) its corresponding spectral analysis (28).

4.2.3. Backscattered Scanning Electron Microscopy (BSEM)

Figure 15a presents an BSEM image of the surface of the runout sample, highlighting the fatigue-induced damage. Cracks are visible in the aggregate particle and cementitious matrix, particularly in the C-S-H gel phases, surrounding nonhydrated cement particles, portlandite crystals, or near pores, which act as stress concentration zones. Some cracks stop propagating and fade out.

Figure 15b shows the spectral analysis of the minerals within the rectangular area in Figure 15a, focusing on a smooth surface identified as a siliceous aggregate particle through spectral analysis. Additional images and analyses, particularly of the interfacial transition zone (ITZ), reveal new C-S-H gel phases overlapping cracks in the ITZ and new hydrated C-S-H phases near a silica fume particle, likely formed by pozzolanic reactions, halting crack propagation (see Figures 10-12 in (28)). A significant aluminum peak suggests the formation of C-A-S-H gels, as previously reported (63–65), which consist of longer silica chains and play a role in halting crack propagation. Additionally, potential portlandite carbonation may form calcite, releasing water into the system (66, 67), further promoting hydration under cyclic compressive loads. Thus, SEM analysis suggests that self-healing under compressive cyclic loading is driven by both hydration of anhydrous phases and pozzolanic reactions forming C-A-S-H gels.

4.2.4. Mercury Intrusion Porosimetry (MIP)

Figure 16 shows the pore size distribution for both specimens, with peaks corresponding to predominant pore sizes that account for higher void volume. Peaks below 1 μm are similarly distributed, but beyond this size, differences emerge. Around 10 μm, the runout specimen exhibits a peak above the control specimen, indicating greater void volume, likely due to crack openings caused during compressive testing. These openings would depend on the damage level of each specimen. Conversely, smaller size differences are more indicative of the concrete matrix’s microstructure. Notably, the runout specimen shows a clear reduction in pore volume around 0.04 μm, and between 1 μm and 5 μm, as seen in the logarithmic plot of injected mercury per sample mass (Figure 16).

Table 4 presents additional MIP analysis results. The runout specimen shows a lower total pore area and average pore diameter compared to the control specimen. Tortuosity, defined as the ratio of actual

flow path length to the straight distance between the path ends, is also reduced, with the runout specimen at 56% of the control’s value. These results suggest a reduction in pore volume and closure of microcracking paths after the application of cyclic compressive loads.

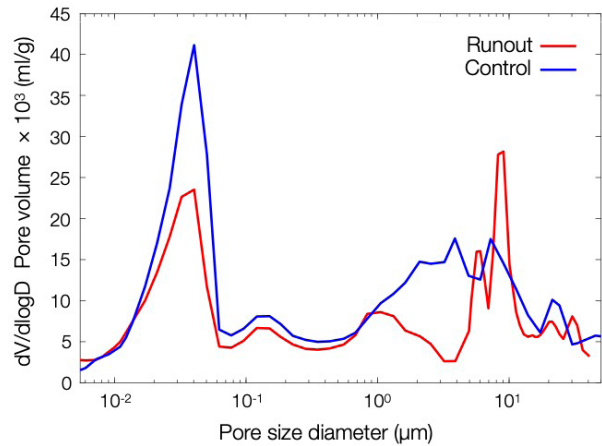


FIGURE 16. Porosimetry of both runout and control specimens (28).

TABLE 4. Parameters obtained by MIP.

Parameter	Runout	Control
Total pore area (m ² /g)	2.23	2.80
Average pore diameter (nm)	55.6	68.4
Tortuosity	5.17	9.18

TABLE 5. Pore size classification in hydrated cement pastes (modified from Mindess and Young (68, 69)).

Type of pore	Denomination	Size
Gel pore	Interlayer micropore	> 0.5 nm
Gel pore	Micropore	0.5 nm-2.5 nm
Gel pore	Small capillary (gel)	2.5 nm-10 nm
Capillary pore	Medium capillary	10 nm-50 nm
Capillary pore	Large capillary	0.05 μm-10 μm
Air	Entrapped air	0.01 mm-1 mm

5. DISCUSSION

The results support the notion that cyclic compressive loads induce an autogenous self-healing process in the material. The primary causes of this phenomenon are analyzed below.

Considering the types of water and voids within the hydrated cement paste is crucial to understanding

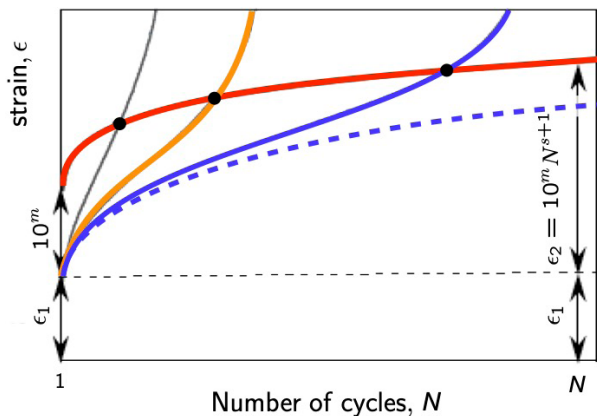


FIGURE 17. Effect of the autogenous self-healing due to fatigue on the cyclic creep curves. Blue curves schematically represent specimens experiencing significant self-healing, thus enduring longer—solid line—or surviving—dashed line—than another specimen of the same material with no or minimal self-healing—orange curve—.

autogenous self-healing in concrete. Capillary water, which is not bound to the solid surface, plays a vital role in the self-healing process. Capillary voids—spaces not filled by hydration products, see Table 5—depend on the degree of hydration (68). For autogenous self-healing to take place, there must be sufficient free water available. The movement of water into cracks is influenced by factors such as porosity, pore structure, and connectivity (Figure 16, Table 4). Although the concrete examined in the previous section has a low water-binder ratio, its short age and humid curing conditions are conducive to potential self-healing.

Cyclic compressive loads exert simultaneous damage and healing effects. Whether healing or damage dominates influences the residual compressive strength and fatigue life (as sketched in Figure 17). As cyclic loads generate microcracks, water moves through them (70, 71), reaching other areas via flow and diffusion (70), as schematically represented in Figure 18. The dynamic pressure from water at crack

tips induces stress, potentially deepening cracks (72). Higher pressure and larger crack openings accelerate microcrack growth, reducing fatigue life if no self-healing occurs (73).

However, self-healing comes about through the hydration of non-hydrated particles in young concrete, while carbonation dominates in older concrete (74). Water movement through cracks (Figure 18) promotes ongoing hydration, carbonation, and dissolution reactions, creating complex chemical processes that influence self-healing (75). Crack morphology affects healing, with faster product formation at crack tips (76).

The primary physical cause of self-healing is the expansion of hydration products near microcracks when exposed to water (77). The main product is CaCO_3 (77), and non-hydrated particles also form portlandite and C-S-H gel. However, C-S-H gel primarily accumulates on crack surfaces, not within cracks (77). Self-healing near crack surfaces is driven by rapid crystalline precipitation. Continuous hydration enhances early-age self-healing due to higher portlandite and moisture content (36), although carbonation may play a greater role (36). These reactions alter concrete’s microstructure, affecting porosity, permeability, and hydration (78, 79).

5.1. Effect of the mineral additions

Mineral additions with pozzolanic activity (e.g., silica fume) participate in hydration, while non-pozzolanic additions (e.g., limestone powder) act as nucleation sites, both contributing to C-S-H gel formation and pore refinement (80, 81). This reduces stress concentrations at defects, which are linked to fractures (80, 82). Mineral additions also enhance autogenous self-healing via delayed hydration, depending on their reactivity during microcracking (36, 83).

Optimal limestone powder content (10%) improves fiber-matrix bonding by increasing C-S-H gel density

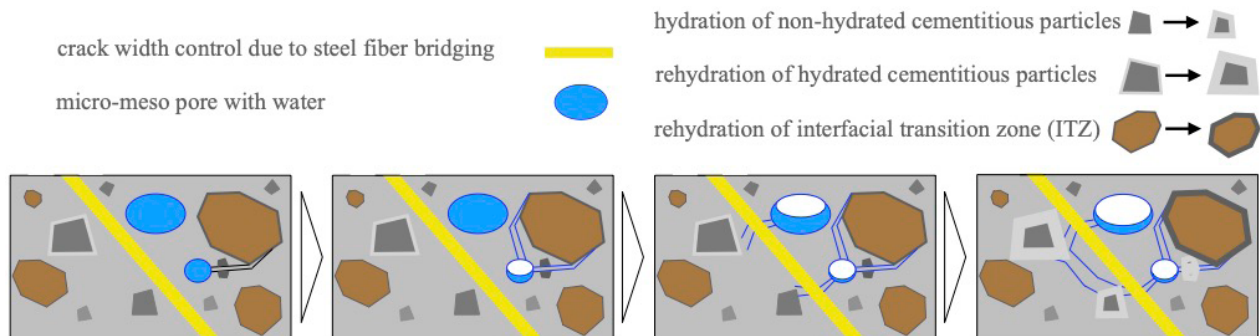


FIGURE 18. Plausible autogenous self-healing mechanisms of cracks in SFRC [28].

and reducing porosity, while excess powder leads to low-density C-S-H, weakening this bond (84). Pozzolanic additions reduce gel porosity but may increase capillary pores due to C-S-H gel carbonation (66). Continued hydration and pozzolanic reactions may promote long-term self-healing at greater depths (77, 85).

5.2. Effect of the carbonation

In carbonation, portlandite —Ca(OH)₂— reacts with CO₂, along with C-S-H gel and unreacted cement, water being essential for these reactions. This process, governed by exposure conditions, alters porosity and pore size distribution, sometimes increasing strength due to structural changes in the C-S-H gel. However, this can lead to carbonation-induced cracking, making it difficult to assess the overall impact on mechanical and transport properties (86). The C-S-H gel, which contains the most calcium, exhibits complex carbonation behavior influenced by the original Ca/Si ratio, CO₂ concentration, and portlandite presence (66, 87).

Using pozzolanic mineral additions, like silica fume as in the case study above (see Table 2), alters the role of portlandite in carbonation. As pozzolanic material increases, portlandite production during hydration decreases, while its consumption in the pozzolanic reaction rises. Adding silica fume may enhance carbonation in concrete, helping to seal cracks. However, DTA and TGA results show that the carbonated phase content is similar in both the reference sample and the one under compressive cyclic loads (see Table 3). Therefore, we do not anticipate that faster carbonation under these loads will significantly improve the self-healing process.

5.3. Effect of the steel fiber reinforcement

Fibers play a crucial role in the autogenous self-healing process under compressive cyclic loads by controlling microcrack width and propagation (88–99). Microcracks narrower than 50 μm may fully seal (88, 100–102). Fiber reinforcement also increases the tortuosity and roughness of microcracks (103), enhancing autogenous self-healing (Figure 18). However, excessive fiber content can introduce weak interfaces, reducing reinforcement effectiveness (14, 80).

Crack opening rate affects internal water pressure distribution: a slower rate allows pressure to build up, while a faster rate prevents the waterfront from advancing along the crack front. When a saturated fracture zone closes rapidly, water can become trapped, acting as a wedge that induces tensile stresses (104).

As tensile stresses increase and crack surfaces begin to separate, the cohesive force of water slows crack initiation and propagation.

5.4. Effect of the damage distribution and size effect

The self-healing process competes with fatigue-induced damage, and understanding their interaction is crucial, as the material response depends on which mechanism dominates (Figure 17). Fatigue damage in cementitious materials primarily arises from the initiation and propagation of microcracks (105). To interpret overall fatigue behavior, including the interfacial transition zone (ITZ), it is important to examine fatigue behavior at different scales.

At the nanoscale, crack propagation is governed by the breaking of nanoparticle connections, particularly the rupture of C-S-H gel, which propagates until merging into the main crack (105). Weakening localized stress concentrations through pore structure refinement or connecting nano-cracks allows a broader distribution of microcracks, promoting energy dissipation. Nano-crack propagation can be slowed by the bonding effect of nano-cracks and by the formation of denser C-S-H gel with higher polymerization, along with smaller calcium hydroxide crystals (70, 80, 106).

At the microscale, existing cracks, especially in the ITZ, coalesce with fatigue cracks in the cement matrix (105). Due to its porosity, the ITZ is highly vulnerable to fatigue, exhibiting a higher likelihood of crack initiation and propagation compared to the matrix (105, 107–109). Faster crack growth in the ITZ accelerates damage, while increased damage distribution enhances autogenous self-healing by generating more microcracks and facilitating energy dissipation, thus strengthening the material.

The internal stress distribution, influenced by specimen size, further affects self-healing potential, as previously noted in Section 3 (26). Scale effects on crack propagation and fatigue life can be analyzed from the micro- to the macroscale (110, 111). From this perspective, smaller specimens result in a more distributed arrangement of microcracks, making them more susceptible to significant self-healing compared to larger specimens of the same material (26, 27).

5.5. Effective time for autogenous self-healing

Autogenous self-healing is induced over a specific period. By 10 hours into hydration, significant amounts of C-S-H gel, portlandite, and ettringite are present, especially the latter. At 50 hours, C-S-H

gel and portlandite increase notably, while ettringite decreases. Calcite content is crucial as it controls available carbonates and influences the formation of hemicarboaluminate phases over ettringite and monosulfate phases (112).

The extent of crack repair depends on the repair type, duration, and crack characteristics. If the volume of cracks is insufficient for complete closure, repair efficiency decreases due to the exponential growth of cracks (113). When damage progresses rapidly, self-healing cannot counteract it, as seen in tests at 90% of the compressive strength in Figure 13, where the longest fatigue life was under one hour. For other loading conditions, the longest fatigue life for fatigue-failed specimens was about eight hours, after which a stable strain phase occurs. Analogously, low frequencies in steel-fiber reinforced concrete fatigue can also favor the self-healing process by providing the time needed for it, as described in subsection 2.3 (17). In summary, slower damage progression increases the likelihood of self-healing controlling crack propagation.

6. CONCLUSIONS

This article examined the effect of size on the compressive fatigue of steel fiber reinforced concrete, described the autogenous self-healing of this material resulting from compressive fatigue, and the interactions between them. Additionally, it included a review of fatigue phenomenology to familiarize the reader with the topic, drawing mainly from the authors' contributions to the state of the art. The research outlined in the paper yielded several relevant conclusions:

- **Role of fibers in fatigue behavior & effect of frequency:** Steel fibers significantly enhance the fatigue life of SFRC, particularly at low to intermediate fiber contents, by improving post-cracking behavior and reducing crack propagation through fiber pull-out mechanisms. However, excessive fiber content can have adverse effects, as it introduces matrix imperfections and air voids, which may serve as crack initiation points. Therefore, there is an optimal fiber dosage, beyond which the benefits of fiber reinforcement decline. Additionally, fibers promote a denser microcrack pattern that evolves gradually, increasing the material's stability and toughness by absorbing the released elastic energy. This controlled evolution of cracks may also allow sufficient time for self-healing processes to take place, particularly under low-frequency loading.
- **Size effect in compressive fatigue:** Specimen size significantly affects the fatigue life

of SFRC. Larger specimens tend to exhibit reduced fatigue life due to the increased likelihood of microcracks and large pores acting as stress concentrators. These microcracks can become unstable because of the large amount of elastic energy available to drive their propagation with each cycle. This behavior aligns with classical size effect theory, where larger elements show lower strength under cyclic loading because of their greater potential for crack growth. Conversely, the confined conditions in smaller specimens, particularly cubes, along with their increased relative capacity for energy dissipation, make them more resistant to fatigue. This phenomenon may interact with fatigue-induced additional hydration, which requires extensive microcracking and time to fully develop, heal, and even improve the material's properties. These insights are essential for scaling fatigue performance from small laboratory specimens to real-world structural elements.

- **Autogenous self-healing:** A key finding is the substantial role of autogenous self-healing in enhancing fatigue resistance. Fatigue-induced microcracks allow occluded moisture to penetrate the concrete matrix, which rehydrates dormant cementitious particles and promotes the precipitation of calcium carbonate. These processes help seal microcracks and improve the material's residual strength. This effect was particularly evident in specimens subjected to fatigue loading that stood prolonged cycles, exhibiting a notable increase in compressive strength post-fatigue. These positive effects are often overlooked in concrete technology, but they present a promising opportunity to harness and leverage the material improvements induced by cyclic loads in SFRC, which is naturally prone to self-healing under fatigue conditions.
- **Interaction between size effect and autogenous self-healing:** The size effect interacts with the self-healing process. Smaller specimens, with more extensive microcracking relative to their volume, provide greater opportunities for self-healing mechanisms to activate. However, the effectiveness of self-healing is contingent on factors such as the availability of unhydrated particles and occluded water.
- **Implications for structural design:** These results have important implications for the design of SFRC in structural applications, particularly for elements subjected to cyclic compressive loads, such as wind turbine towers and high-speed railway slabs. The size effect must be accounted for in fatigue design, and the potential

for autogenous self-healing should be considered as a factor that can enhance long-term durability.

Overall, this research highlights the complex interaction between fatigue loading, size effect, fiber reinforcement, and autogenous self-healing in SFRC. It underscores the need for careful consideration of these phenomena in both material design and the scaling of experimental results to full-scale structural elements.

Funding Sources

The authors acknowledge the funding obtained from the *Ministerio de Ciencia e Innovación* through the project PID2019-110928RB-C31 and PID2023-147971OB-C31, and from the *Universidad de Castilla-La Mancha*, Spain, and the *Fondo Europeo de Desarrollo Regional* through grant 2022-GRIN-34124.

Authorship contribution statement

Gonzalo Ruiz: Conceptualization, Methodology, Experiments, Calculations, Writing – original draft, Writing – review & editing, Supervision, Resources, Funding acquisition.

Ángel De La Rosa: Methodology, Experiments, Calculations, Writing – original draft, Writing – review & editing.

José Joaquín Ortega: Methodology, Experiments, Calculations, Writing – original draft, Writing – review & editing.

Elisa Poveda: Methodology, Experiments, Calculations, Writing – review & editing.

Rena C. Yu: Methodology, Experiments, Calculations, Writing – review & editing.

Manuel Tarifa: Methodology, Experiments, Calculations, Writing – review & editing.

Xiaoxin X. Zhang: Methodology, Experiments, Calculations, Writing – review & editing.

Lucía Garrijo: Methodology, Experiments, Calculations, Writing – review & editing.

Declaration of competing interest

The authors of this article declare that they have no financial, professional or personal conflicts of interest that could have inappropriately influenced this work.

REFERENCES

- Bažant ZP, Planas J. 1998. Fracture and size effect in concrete and other quasibrittle materials. CRC Press, Boca Raton, Florida, USA.
- Del Viso JR, Carmona JR, Ruiz G. 2008. Shape and size effects on the compressive strength of high-strength concrete. *Cem. Concr. Res.* 38(3):386-395. <https://doi.org/10.1016/j.cemconres.2007.09.020>
- Jansen DC, Shah SP. 1997. Effect of length on compressive strain softening of concrete. *J. Eng. Mech.* 123(1):25-35. [https://doi.org/10.1061/\(ASCE\)0733-9399\(1997\)123:1\(25\)](https://doi.org/10.1061/(ASCE)0733-9399(1997)123:1(25))
- Wu B, Liu C, Yang Y. 2013. Size effect on compressive behaviours of normal-strength concrete cubes made from demolished concrete blocks and fresh concrete. *Mag. Concr. Res.* 65(19):1155-1167. <https://doi.org/10.1680/mac.13.00053>
- Sim JI, Yang KH, Jeon JK. 2013. Influence of aggregate size on the compressive size effect according to different concrete types. *Constr. Build. Mater.* 44:716-725. <https://doi.org/10.1016/j.conbuildmat.2013.03.066>
- Paris P, Erdogan F. 1963. A critical analysis of crack propagation laws. *J. Basic Eng.* 85(4):528-533. <https://doi.org/10.1115/1.3656900>
- Zhang J, Li VC, Stang H. 2001. Size effect on fatigue in bending of concrete. *J. Mater. Civ. Eng.* 13(6):446-453. [https://doi.org/10.1061/\(ASCE\)0899-1561\(2001\)13:6\(446\)](https://doi.org/10.1061/(ASCE)0899-1561(2001)13:6(446))
- Taher SEDF, Fawzy TM. 2000. Performance of very-high-strength concrete subjected to short-term repeated loading. *Mag. Concr. Res.* 52(3):219-223. <https://doi.org/10.1680/mac.2000.52.3.219>
- Sinaie S, Heidarpour A, Zhao XL, Sanjayan JG. 2015. Effect of size on the response of cylindrical concrete samples under cyclic loading. *Constr. Build. Mater.* 84:399-408. <https://doi.org/10.1016/j.conbuildmat.2015.03.076>
- Di Prisco M, Plizzari G, Vandewalle L. 2009. Fibre reinforced concrete: new design perspectives. *Mater. Struct.* 42:1261-1281. <https://doi.org/10.1617/s11527-009-9529-4>
- Masih VW, Ruiz G, Yu RC, De La Rosa A. 2024. Crack initiation and growth in indirect tensile tests of steel fiber-reinforced concrete studies by means of DIC. In: Mechtcherine V, Signorini C, Junger D, editors. *Transforming Construction: Advances in Fiber Reinforced Concrete*, BEFIB 2024. RILEM Bookseries 54. p. 43-50.
- Ruiz G, De La Rosa A, Poveda E, Zanon R, Schäfer M, Wolf S. 2023. Compressive behaviour of steel-fibre reinforced concrete in Annex L of new Eurocode 2. *Hormigón y Acero.* 299-300:187-198. <https://doi.org/10.33586/hya.2022.3092>
- Carmona JR, Cortés-Buitrago R, Rey-Rey J, Ruiz G. 2022. Planar crack approach to evaluate the flexural strength of fiber-reinforced concrete sections. *Materials.* 15(17):5821. <https://doi.org/10.3390/ma15175821>
- Poveda E, Ruiz G, Cifuentes H, Yu RC, Zhang XX. 2017. Influence of the fiber content on the compressive low-cycle fatigue behavior of self-compacting SFRC. *Int. J. Fatigue.* 101(1):9-17. <https://doi.org/10.1016/j.ijfatigue.2017.04.005>
- Morris AD, Garrett GG. 1981. A comparative study of the static and fatigue behaviour of plain and steel fibre reinforced mortar in compression and direct tension. *Int. J. Cem. Compos. Lightw. Concr.* 3(2):73-91.
- Lee MK, Barr BIG. 2004. An overview of the fatigue behaviour of plain and fibre reinforced concrete. *Cem. Concr. Compos.* 26(4):299-305. [https://doi.org/10.1016/S0958-9465\(02\)00139-7](https://doi.org/10.1016/S0958-9465(02)00139-7)
- Medeiros A, Zhang XX, Ruiz G, Yu RC, Velasco MSL. 2015. Effect of the loading frequency on the compressive fatigue behavior of plain and fiber reinforced concrete. *Int. J. Fatigue.* 70:342-350. <https://doi.org/10.1016/j.ijfatigue.2014.08.005>
- Li VC, Lin Z, Matsumoto T. 1998. Influence of fiber bridging on structural size-effect. *Int. J. Solids Struct.* 35(31-32):4223-4238. [https://doi.org/10.1016/S0020-7683\(97\)00311-9](https://doi.org/10.1016/S0020-7683(97)00311-9)

19. Fládr J, Bily P. 2018. Specimen size effect on compressive and flexural strength of high-strength fibre-reinforced concrete containing coarse aggregate. *Compos. Part B-Eng.* 138:77-86. <https://doi.org/10.1016/j.compositesb.2017.11.032>
20. Nelson EL, Carrasquillo RL, Fowler DW. 1988. Behavior and failure of high-strength concrete subjected to biaxial-cyclic compression loading. *ACI Mater. J.* 85(4):248-253.
21. Talierto ALF, Gobbi E. 1997. Effect of elevated triaxial cyclic and constant loads on the mechanical properties of plain concrete. *Mag. Concr. Res.* 49(181):353-365. <https://doi.org/10.1680/mac.1997.49.181.353>
22. Cachim PB, Figueiras JA, Pereira PAA. 2002. Fatigue behavior of fiber-reinforced concrete in compression. *Cem. Concr. Compos.* 24(2):211-217. [https://doi.org/10.1016/S0958-9465\(01\)00019-1](https://doi.org/10.1016/S0958-9465(01)00019-1)
23. Malek A, Scott A, Pampanin S, MacRae G, Marx S. 2018. Residual capacity and permeability-based damage assessment of concrete under low-cycle fatigue. *J. Mater. Civ. Eng.* 30(6):04018081. [https://doi.org/10.1061/\(ASCE\)MT.1943-5533.0002248](https://doi.org/10.1061/(ASCE)MT.1943-5533.0002248)
24. Qiu J, Aw-Yong WL, Yang EH. 2018. Effect of self-healing on fatigue of engineered cementitious composites (ECCs). *Cem. Concr. Compos.* 94:145-152. <https://doi.org/10.1016/j.cemconcomp.2018.09.007>
25. Garijo L, Ortega JJ, Ruiz G, De La Rosa A, Zhang XX. 2022. Effect of loading frequency on the fatigue life in compression of natural hydraulic lime mortars. *Theor. Appl. Fract. Mech.* 118:103201. <https://doi.org/10.1016/j.tafmec.2021.103201>
26. Ortega JJ, Ruiz G, Poveda E, González DC, Tarifa M, Zhang X, Yu RC, Vicente MÁ, De La Rosa A. 2022. Size effect on the compressive fatigue of fibre-reinforced concrete. *Constr. Build. Mater.* 322:126238. <https://doi.org/10.1016/j.conbuildmat.2021.126238>
27. González DC, Mena A, Ruiz G, Ortega JJ, Poveda E, Mínguez J, Yu R, De La Rosa A, Vicente MÁ. 2023. Size effect of steel fiber-reinforced concrete cylinders under compressive fatigue loading: Influence of the mesostructure. *Int. J. Fatigue.* 167(B):107353. <https://doi.org/10.1016/j.ijfatigue.2022.107353>
28. De La Rosa A, Ortega JJ, Ruiz G, García Calvo JL, Rubiano Sánchez FJ, Castillo A. 2023. Autogenous self-healing induced by compressive fatigue in self-compacting steel-fiber reinforced concrete. *Cem. Concr. Res.* 173:107278. <https://doi.org/10.1016/j.cemconres.2023.107278>
29. Ferrara L, Krelani V, Moretti F, Roig Flores M, Serna Ros P. 2017. Effects of autogenous healing on the recovery of mechanical performance of high performance fibre reinforced cementitious composites (HPFRCCs): Part 1. *Cem. Concr. Compos.* 83:76-100. <https://doi.org/10.1016/j.cemconcomp.2017.07.010>
30. Mihashi H, Nishiwaki T. 2012. Development of engineered self-healing and self-repairing concrete-State-of-the-art report. *J. Adv. Concr. Technol.* 10(5):170-184. <https://doi.org/10.3151/jact.10.170>
31. Van Tittelboom K, De Belie N. 2013. Self-healing in cementitious materials—A review. *Materials.* 6(6):2182-2217. <https://doi.org/10.3390/ma6062182>
32. De Belie N, Gruyaert E, Al-Tabbaa A, Antonaci P, Baera C, Bajare D, Darquennes A, Davies R, Ferrara L, Jefferson T, Litina C, Miljevic B, Otlewska A, Ranogajec J, Roig-Flores M, Paine K, Lukowski P, Serna P, Tulliani JM, Vucetic S, Wang J, Jonkers HM. 2018. A review of self-healing concrete for damage management of structures. *Adv. Mater. Interfaces.* 5(17):1800074. <https://doi.org/10.1002/admi.201800074>
33. Wu M, Johannesson B, Geiker M. 2012. A review: Self-healing in cementitious materials and engineered cementitious composite as a self-healing material. *Constr. Build. Mater.* 28(1):571-583. <https://doi.org/10.1016/j.conbuildmat.2011.08.086>
34. De Rooij M, Van Tittelboom K, De Belie N, Schlangen E, editors. 2013. Self-healing phenomena in cement-based materials. RILEM Tech. Comm. 221-SHC. Vol. 11. Springer, Dordrecht.
35. Edvardsen C. 1999. Water permeability and autogenous healing of cracks in concrete. *ACI Mater. J.* 96(4):448-454. <https://doi.org/10.14359/645>
36. Roig-Flores M, Formagini S, Serna P. 2021. Self-healing concrete: What is it good for? *Mater. Construcc.* 71(341):e237. <https://doi.org/10.3989/mc.2021.07320>
37. Moreira TNC, Krelani V, Rocha Ferreira S, Ferrara L, Toledo Filho RD. 2022. Self-healing of slag-cement ultra-high performance steel fiber reinforced concrete (uhpfr) containing sisal fibers as healing conveyor. *J. Build. Eng.* 54:104638. <https://doi.org/10.1016/j.job.2022.104638>
38. Snoeck D, De Belie N. 2016. Repeated autogenous healing in strain-hardening cementitious composites by using superabsorbent polymers. *J. Mater. Civ. Eng.* 28(1):1-11. [https://doi.org/10.1061/\(ASCE\)MT.1943-5533.0001360](https://doi.org/10.1061/(ASCE)MT.1943-5533.0001360)
39. Chacón C, Cifuentes H, Luna-Galiano Y, Ríos JD, Ariza P, Leiva C. 2023. Exploring the impact of graphene oxide on mechanical and durability properties of mortars incorporating demolition waste: Micro and nano-pore structure effects. *Mater. Construcc.* 73(352):e327. <https://doi.org/10.3989/mc.2023.351623>
40. Suescum-Morales D, Ríos JD, Martínez De La Concha A, Cifuentes H, Jiménez JR, Fernández JM. 2021. Effect of moderate temperatures on compressive strength of ultra-high-performance concrete: A microstructural analysis. *Cem. Concr. Res.* 140:106303. <https://doi.org/10.1016/j.cemconres.2020.106303>
41. Tarifa M, Zhang XX, Ruiz G, Poveda E. 2015. Full-scale fatigue tests of precast reinforced concrete slabs for railway tracks. *Eng. Struct.* 100:610-621. <https://doi.org/10.1016/j.engstruct.2015.06.016>
42. Poveda E, Yu RC, Lancha JC, Ruiz G. 2015. A numerical study on the fatigue life design of concrete slabs for railway tracks. *Eng. Struct.* 100:455-467. <https://doi.org/10.1016/j.engstruct.2015.06.037>
43. Zanon R, Schäfer M, Ruiz G, Yu RC, De La Rosa A, Masih VW. 2024. Experimental bending tests on encased steel-concrete composite beams with SFRC. In: Mechtcherine V, Signorini C, Junger D, editors. *Transforming Construction: Advances in Fiber Reinforced Concrete*, BEFIB 2024. RILEM Bookseries 54. p. 197-204.
44. Jinawath P. 1974. Cumulative fatigue damage of plain concrete in compression [Ph.D. thesis]. University of Leeds, Leeds, United Kingdom.
45. Holmen JO. 1979. Fatigue of concrete by constant and variable amplitude loading [Ph.D. thesis]. University of Trondheim, Trondheim, Norway.
46. Hordijk DA, Reinhardt HW. 1993. Numerical and experimental investigation into the fatigue behavior of plain concrete. *Exp. Mech.* 33(4):278-285. <https://doi.org/10.1007/BF02322142>
47. Petryna YS, Pfanner D, Stangenberg F, Krätzig WB. 2002. Reliability of reinforced concrete structures under fatigue. *Reliab. Eng. Syst. Saf.* 77(3):253-261. [https://doi.org/10.1016/S0951-8320\(02\)00058-3](https://doi.org/10.1016/S0951-8320(02)00058-3)
48. Zanuy C, de la Fuente P, Albajar L. 2007. Effect of fatigue degradation of the compression zone of concrete in reinforced concrete sections. *Eng. Struct.* 29(11):2908-2920. <https://doi.org/10.1016/j.engstruct.2007.01.030>
49. American Concrete Institute (ACI). 2022. Concrete structure design for fatigue loading--Report. ACI PRC-215-21. American Concrete Institute.
50. Ruiz G, De La Rosa A, Poveda E. 2019. Relationship between residual flexural strength and compression strength in steel-fiber reinforced concrete within the new Eurocode 2 regulatory framework. *Theor. Appl. Fract. Mech.* 103:102310. <https://doi.org/10.1016/j.tafmec.2019.102310>
51. De La Rosa A, Ruiz G, Poveda E. 2019. Study of the compression behavior of steel-fiber reinforced concrete by means of the response surface methodology. *Appl. Sci.* 9(24):5330.

52. Sparks PR, Menzies JB. 1973. Effect of rate of loading upon static and fatigue strengths of plain concrete in compression. *Mag. Concr. Res.* 25(83):73-80. <https://doi.org/10.1680/mac.1973.25.83.73>
53. Lohaus L, Oneschkow N, Wefer M. 2012. Design model for the fatigue behaviour of normal-strength, high-strength and ultra-high-strength concrete. *Struct. Concr.* 13(3):182-192. <https://doi.org/10.1002/suco.201100054>
54. Comité Euro-International du Béton (CEB). 1988. Fatigue of concrete structures. State of the art report. CEB Report 188, Lausanne.
55. fib Bulletins 65 & 66. 2012. Model Code 2010, Final Draft. International Federation for Structural Concrete (fib), Lausanne, Switzerland.
56. Ortega JJ, Ruiz G, Yu RC, Afanador-García N, Tarifa M, Poveda E, Zhang X, Evangelista F. 2018. Number of tests and corresponding error in concrete fatigue. *Int. J. Fatigue.* 116:210-219. <https://doi.org/10.1016/j.ijfatigue.2018.06.022>
57. Tarifa M, Ruiz G, Poveda E, Zhang XX, Vicente MA, González DC. 2018. Effect of uncertainty on load position in the fatigue life of steel-fiber reinforced concrete under compression. *Mater. Struct.* 51(1). <https://doi.org/10.1617/s11527-018-1155-6>
58. González DC, Mena-Alonso Á, Poveda E, Mínguez J, De La Rosa Á, Yu RC, Ruiz G, Vicente MA. 2024. Study of the edge effect in fiber-reinforced concrete cylindrical molded specimens using computed tomography. In: Mechtcherine V, Signorini C, Junger D, editors. *Transforming Construction: Advances in Fiber Reinforced Concrete*, BEFIB 2024. RILEM Bookseries 54. p. 27-34.
59. Saucedo L, Yu RC, Medeiros A, Zhang XX, Ruiz G. 2013. A probabilistic fatigue model based on the initial distribution to consider frequency effect in plain and fiber reinforced concrete. *Int. J. Fatigue.* 48:308-318. <https://doi.org/10.1016/j.ijfatigue.2012.11.013>
60. Blasón S, Poveda E, Ruiz G, Cifuentes H, Fernández Canteli A. 2019. Twofold normalization of the cyclic creep curve of plain and steel-fiber reinforced concrete and its application to predict fatigue failure. *Int. J. Fatigue.* 120:215-227. <https://doi.org/10.1016/j.ijfatigue.2018.11.021>
61. Blasón S, Fernández Canteli A, Poveda E, Ruiz G, Yu RC, Castillo E. 2022. Damage evolution and probabilistic strain-lifetime assessment of plain and fiber-reinforced concrete under compressive fatigue loading: Dual and integral phenomenological model. *Int. J. Fatigue.* 158:106739. <https://doi.org/10.1016/j.ijfatigue.2022.106739>
62. Scrivener K, Snellings R, Lothenbach B, editors. 2016. *A practical guide to microstructural analysis of cementitious materials*. CRC Press, Taylor & Francis Group. ISBN-13: 978-1-4987-3867-5.
63. García Calvo JL, Hidalgo A, Alonso C, Fernández Luco L. 2010. Development of low-pH cementitious materials for HLRW repositories resistance against ground waters aggression. *Cem. Concr. Res.* 40(8):1290-1297. <https://doi.org/10.1016/j.cemconres.2009.11.008>
64. García Calvo JL, Sánchez Moreno M, Alonso Alonso MC, Hidalgo López A, García Olmo J. 2013. Study of the microstructure evolution of low-pH cements based on ordinary Portland cement (OPC) by mid- and near-infrared spectroscopy, and their influence on corrosion of steel reinforcement. *Materials.* 6(6):2508-2521. <https://doi.org/10.3390/ma6062508>
65. Fernández A, Alonso MC, García-Calvo JL, Lothenbach B. 2016. Influence of the synergy between mineral additions and Portland cement in the physical-mechanical properties of ternary binders. *Mater. Construcc.* 66(324). <https://doi.org/10.3989/mc.2016.10815>
66. Von Greve-Dierfeld S, Lothenbach B, Vollpracht A, Wu B, Huet B, Andrade C, Medina C, Thiel C, Gruyaert E, Vanoutrive H, et al. 2020. Understanding the carbonation of concrete with supplementary cementitious materials: A critical review by RILEM TC 281-CCC. *Mater. Struct.* 53(6):136. <https://doi.org/10.1617/s11527-020-01558-w>
67. Morandea A, Tognazzi C, Dangla P. 2014. Investigation of the carbonation mechanism of CH and C-S-H in terms of kinetics, microstructure changes and moisture properties. *Cem. Concr. Res.* 56:153-170. <https://doi.org/10.1016/j.cemconres.2013.11.015>
68. Ye G. 2003. Experimental study and numerical simulation of the development of the microstructure and permeability of cementitious materials [Ph.D. thesis]. T.U. Delft, Delft University Press.
69. Mindess S, Young J. 1981. *Concrete*. Prentice-Hall Civil Engineering and Engineering Mechanics Series. Prentice-Hall.
70. Wang L, Zhang W. 2021. Investigation on water absorption in concrete after subjected to compressive fatigue loading. *Constr. Build. Mater.* 299:123897. <https://doi.org/10.1016/j.conbuildmat.2021.123897>
71. Lei B, Li W, Li Z, Wang G, Sun Z. 2018. Effect of cyclic loading deterioration on concrete durability: Water absorption, freeze-thaw, and carbonation. *J. Mater. Civ. Eng.* 30(9):04018220. [https://doi.org/10.1061/\(ASCE\)MT.1943-5533.0002450](https://doi.org/10.1061/(ASCE)MT.1943-5533.0002450)
72. Sun X, Tian Y, Yin W, Wang H. 2022. Effect of free water on fatigue performance of concrete subjected to compressive cyclic load. *Constr. Build. Mater.* 318:125995. <https://doi.org/10.1016/j.conbuildmat.2021.125995>
73. Zhang Y, Zhang S, Wei G, Wei X, Jin L, Xu K. 2019. Water transport in unsaturated cracked concrete under pressure. *Adv. Civ. Eng.* 2019(1):4504892. <https://doi.org/10.1155/2019/4504892>
74. Van Tittelboom K, De Belie N. 2013. Self-healing in cementitious materials—A review. *Materials.* 6(6):2182-2217. <https://doi.org/10.3390/ma6062182>
75. Yang S, Yang Y, Caggiano A, Ukrainczyk N, Koenders E. 2022. A phase-field approach for portlandite carbonation and application to self-healing cementitious materials. *Mater. Struct.* 55(46). <https://doi.org/10.1617/s11527-022-01887-y>
76. Yang S, Aldakheel F, Caggiano A, Wriggers P, Koenders E. 2020. A review on cementitious self-healing and the potential of phase-field methods for modeling crack-closing and fracture recovery. *Materials.* 13(22):5265. <https://doi.org/10.3390/ma13225265>
77. Yao C, Shen A, Guo Y, Lyu Z, He Z, Wu H. 2022. A review on autogenous self-healing behavior of ultra-high performance fiber reinforced concrete (UHPC). *Arch. Civ. Mech. Eng.* 22(145). <https://doi.org/10.1007/s43452-022-00462-0>
78. Javierre E, Gaspar F, Rodrigo C. 2019. Modelling the carbonation reactions in self-healing concrete. In: 10th International Conference on Fracture Mechanics of Concrete and Concrete Structures, FraMCoS-X. <https://doi.org/10.21012/FC10.235637>
79. Chitez A, Jefferson A. 2016. A coupled thermo-hygro-chemical model for characterising autogenous healing in ordinary cementitious materials. *Cem. Concr. Res.* 88:184-197. <https://doi.org/10.1016/j.cemconres.2016.07.002>
80. Li L, Xu L, Huang L, Xu F, Huang Y, Cui K, Zeng Y, Chi Y. 2022. Compressive fatigue behaviors of ultra-high performance concrete containing coarse aggregate. *Cem. Concr. Compos.* 128:104425. <https://doi.org/10.1016/j.cemconcomp.2022.104425>
81. Golewski G, Szostak B. 2021. Strengthening the very early-age structure of cementitious composites with coal fly ash via incorporating a novel nanoadmixture based on C-S-H phase activators. *Constr. Build. Mater.* 312:125426. <https://doi.org/10.1016/j.conbuildmat.2021.125426>
82. Golewski G. 2018. An analysis of fracture toughness in concrete with fly ash addition considering all models of cracking. *IOP Conf. Ser.: Mater. Sci. Eng.* 416:012029. <https://doi.org/10.1088/1757-899X/416/1/012029>
83. Jaroenratanirom D, Sahamitmongkol R. 2011. Self-crack closing ability of mortar with different additives. *J. Met. Mater. Miner.* 21(1):9-17.
84. Zhuang W, Li S, Wang Z, Zhang Z, Yu Q. 2022. Impact of micromechanics on dynamic compressive behavior of ultra-

- high performance concrete containing limestone powder. *Compos. Part B-Eng.* 243:110160. <https://doi.org/10.1016/j.compositesb.2022.110160>
85. Fan S, Li M. 2015. X-ray computed microtomography of three-dimensional microcracks and self-healing in engineered cementitious composites. *Smart Mater. Struct.* 24:015021. <https://doi.org/10.1088/0964-1726/24/1/015021>
 86. Savija B, Luković M. 2016. Carbonation of cement paste: Understanding, challenges, and opportunities. *Constr. Build. Mater.* 117:285-301. <https://doi.org/10.1016/j.conbuildmat.2016.04.138>
 87. Visser J. 2014. Influence of the carbon dioxide concentration on the resistance to carbonation of concrete. *Constr. Build. Mater.* 67(A):8-13. <https://doi.org/10.1016/j.conbuildmat.2013.11.005>
 88. Cuenca E, Tejedor A, Ferrara L. 2018. A methodology to assess crack-sealing effectiveness of crystalline admixtures under repeated cracking-healing cycles. *Constr. Build. Mater.* 179:619-632. <https://doi.org/10.1016/j.conbuildmat.2018.05.261>
 89. Van Tittelboom K, Gruyaert E, Rahier H, De Belie N. 2012. Influence of mix composition on the extent of autogenous crack healing by continued hydration or calcium carbonate formation. *Constr. Build. Mater.* 37:349-359. <https://doi.org/10.1016/j.conbuildmat.2012.07.026>
 90. Ferrara L, Krelani V, Moretti F, Roig-Flores M, Serna Ros P. 2017. Effects of autogenous healing on the recovery of mechanical performance of high performance fibre reinforced cementitious composites (HPFRCCs): Part 1. *Cem. Concr. Compos.* 83:76-100. <https://doi.org/10.1016/j.cemconcomp.2017.07.010>
 91. Ferrara L, Krelani V, Moretti F. 2016. Autogenous healing on the recovery of mechanical performance of High Performance Fibre Reinforced Cementitious Composites (HPFRCCs): Part 2 - correlation between healing of mechanical performance and crack sealing. *Cem. Concr. Compos.* 73:299-315. <https://doi.org/10.1016/j.cemconcomp.2016.08.003>
 92. Roig-Flores M, Moscato S, Serna P, Ferrara L. 2015. Self-healing capability of concrete with crystalline admixtures in different environments. *Constr. Build. Mater.* 86:1-11. <https://doi.org/10.1016/j.conbuildmat.2015.03.091>
 93. Ferrara L, Ferreira S, Krelani V, Della Torre M, Silva F, Toledo R. 2015. Natural fibers as promoters of autogenous healing in HPFRCCs: Results from ongoing Brazil-Italy cooperation. *fib Bulletin* 305.
 94. Cuenca E, Echegaray-Oviedo J, Serna P. 2015. Influence of concrete matrix and type of fiber on the shear behavior of self-compacting fiber reinforced concrete beams. *Compos. Part B-Eng.* 75:135-147. <https://doi.org/10.1016/j.compositesb.2015.01.037>
 95. Snoeck D, De Belie N. 2015. From straw in bricks to modern use of microfibers in cementitious composites for improved autogenous healing—A review. *Constr. Build. Mater.* 95:774-787. <https://doi.org/10.1016/j.conbuildmat.2015.07.018>
 96. Wu M, Johannesson B, Geiker M. 2012. Self-healing in cementitious materials and engineered cementitious composite as a self-healing material: A review. *Constr. Build. Mater.* 28(1):571-583. <https://doi.org/10.1016/j.conbuildmat.2011.08.086>
 97. Ortiz-Navas F, Navarro-Gregori J, Leiva-Herdocia G, Serna P, Cuenca E. 2018. An experimental study on the shear behaviour of reinforced concrete beams with macro-synthetic fibres. *Constr. Build. Mater.* 169:888-899. <https://doi.org/10.1016/j.conbuildmat.2018.02.023>
 98. Susetyo J, Vecchio F. 2010. Effectiveness of the steel fiber as minimum shear reinforcement: panel test. *fib Bulletin* 57:227-241. <https://doi.org/10.35789/fib.BULL.0057.Ch14>
 99. Cuenca E, Serna P. 2013. Shear behavior of prestressed precast beams made of self-compacting fiber reinforced concrete. *Constr. Build. Mater.* 45:145-156. <https://doi.org/10.1016/j.conbuildmat.2013.03.096>
 100. Yang Y, Lepech M, Yang EH, Li VC. 2009. Autogenous healing of engineered cementitious composites under wet-dry cycles. *Cem. Concr. Res.* 39(5):382-390. <https://doi.org/10.1016/j.cemconres.2009.01.013>
 101. Snoeck D, Van Tittelboom K, Steuperaet S, Dubrue P, De Belie N. 2014. Self-healing cementitious materials by the combination of microfibers and superabsorbent polymers. *J. Intell. Mater. Syst. Struct.* 25(1):13-24. <https://doi.org/10.1177/1045389X12438623>
 102. Li VC, Wang S, Wu C. 2001. Tensile strain-hardening behavior of polyvinyl alcohol engineered cementitious composites (PVA-ECC). *ACI Mater. J.* 98(6):483-492. <https://doi.org/10.14359/10851>
 103. Picandet V, Khelidj A, Bellegou. 2009. Crack effects on gas and water permeability of concretes. *Cem. Concr. Res.* 39(6):537-547. <https://doi.org/10.1016/j.cemconres.2009.03.009>
 104. Slowik V, Saouma V. 2000. Water pressure in propagating concrete cracks. *J. Struct. Eng.* 126(2):235-242. [https://doi.org/10.1061/\(ASCE\)0733-9445\(2000\)126:2\(235\)](https://doi.org/10.1061/(ASCE)0733-9445(2000)126:2(235))
 105. Gan Y, Zhang H, Zhang Y, Xu Y, Schlangen E, van Breugel K, Savija B. 2021. Experimental study of flexural fatigue behaviour of cement paste at the microscale. *Int. J. Fatigue.* 151:106378. <https://doi.org/10.1016/j.ijfatigue.2021.106378>
 106. Cui X, Han B, Zheng Q, Yu X, Dong S, Zhang L, Ou J. 2017. Mechanical properties and reinforcing mechanisms of cementitious composites with different types of multiwalled carbon nanotubes. *Compos. Part A: Appl. Sci. Manuf.* 103:131-147. <https://doi.org/10.1016/j.compositesa.2017.10.001>
 107. Gan Y, Zhang H, Liang M, Zhang Y, Schlangen E, van Breugel K, Savija B. 2022. Flexural strength and fatigue properties of interfacial transition zone at the microscale. *Cem. Concr. Compos.* 133:104717. <https://doi.org/10.1016/j.cemconcomp.2022.104717>
 108. Toumi A, Bascoul A, Turatsinze A. 1998. Crack propagation in concrete subjected to flexural cyclic loading. *Mater. Struct.* 31:451-458. <https://doi.org/10.1007/BF02480468>
 109. Saito M. 1987. Characteristics of microcracking in concrete under static and repeated tensile loading. *Cem. Concr. Res.* 17(2):211-218. [https://doi.org/10.1016/0008-8846\(87\)90104-9](https://doi.org/10.1016/0008-8846(87)90104-9)
 110. Bažant ZP, Xu KM. 1991. Size effect in fatigue fracture of concrete. *ACI Mater. J.* 88(4):390-399.
 111. Kirane K, Bažant ZP. 2016. Size effect in Paris law and fatigue lifetimes for quasibrittle materials: Modified theory, experiments and micro-modeling. *Int. J. Fatigue.* 83(2):209-220. <https://doi.org/10.1016/j.ijfatigue.2015.10.015>
 112. Bullard J, Lothenbach B, Stutzman P, Snyder K. 2011. Coupling thermodynamics and digital image models to simulate hydration and microstructure development of portland cement pastes. *J. Mater. Res.* 26(4):609-622. <https://doi.org/10.1557/jmr.2010.41>
 113. Grossegger D. 2021. Fatigue damage self-healing analysis and the occurrence of an optimal self-healing time in asphalt concrete. *J. Mater. Civ. Eng.* 33(6). [https://doi.org/10.1061/\(ASCE\)MT.1943-5533.0003717](https://doi.org/10.1061/(ASCE)MT.1943-5533.0003717)